https://doi.org/10.5194/egusphere-2026-4785
Preprint. Discussion started: 28 August 2026

Volcanically Forced Cooling over the last 600 years in Northern Patagonia

Rob Wilson[1], Ignacio Mundo[2,3], Lauren Marshall[1,4], Emily Reid[1], Michael Sigl[5], Anja Schmidt[6,7,8], Claudia Timmreck[9], Shih-Wei Fang[10,], Rory Abernethy[11], Valerie Daux[12], and Ricardo Villalba[2]

[1] School of Earth & Environmental Sciences, University of St. Andrews, St. Andrews, UK
[2] Laboratorio de Dendrocronología e Historia Ambiental, IANIGLA-CONICET, Mendoza, Argentina
[3] Facultad de Ciencias Exactas y Naturales, Universidad Nacional de Cuyo, Mendoza, Argentina
[4] Department of Earth Sciences, Durham University, Durham, UK
[5] Climate and Environmental Physics & Oeschger Centre for Climate Change Research, University of Bern, Bern, Switzerland
[6] Institute of Atmospheric Physics (IPA), German Aerospace Center (DLR), Oberpfaffenhofen, Germany
[7] Meteorological Institute, Ludwig Maximilian University of Munich, Munich, Germany
[8] Yusuf Hamied Department of Chemistry, University of Cambridge, Cambridge, United Kingdom
[9] Max Planck Institute for Meteorology, Hamburg, Germany
[10] Department of Atmospheric Sciences, National Central University, Taoyuan, 320317, Taiwan
[11] Biological and Environmental Sciences, University of Stirling, Stirling, UK
[12] Laboratoire des Sciences du climat et de l'Environnement, CNRS-CEA-UVSQ-Université Paris-Saclay, Gif-sur-Yvette, France

Correspondence to: Rob Wilson (rjsw@st-andrews.ac.uk)

Abstract. We present the first tree-ring (TR) based summer surface temperature reconstruction (1382-2017) for the Southern Hemisphere that expresses strong volcanically forced cooling. The Northern Patagonia (NPAT) reconstruction is based on ring-width (RW) and Blue Intensity (BI) parameters measured from *Araucaria araucana* trees sampled from 6 locations across the middle to southern end of the species' range in Argentina. This multi-TR-parameter reconstruction explains 53% of the summer surface temperature variance (1903-2017), which is on par with the fidelity of density or mixed TR parameter-based reconstructions from the Northern Hemisphere. The reconstruction coheres strongly with surface mean air temperatures for a large region in South America, including sea surface temperatures well into the southeastern Pacific. The warmest 10-year period is 2008-2017, corresponding to the last ten years of the reconstruction, while the coldest period is 1455-1464. The coldest reconstructed austral summer is 1971, followed by 1460. For both the NPAT reconstruction and a range of model simulations, superposed epoch analysis, using significant tropical eruptions since the 1400s, indicates a significant post-eruption T+1 mean surface cooling of ca. 0.4 - 1.0 ºC, depending on which volcanic events are used. The degree of relative cooling is on par, or even stronger, with the cooling represented by individual TR records used in the Northern Hemisphere N-TREND reconstruction suggesting that the volcanic response in northern Patagonia over the last 6 centuries is equivalent, or even more extreme, to what is observed in many Northern Hemisphere locations. Our results

https://doi.org/10.5194/egusphere-2026-4785
Preprint. Discussion started: 28 August 2026

indicate that the use of ring-density parameters is of paramount importance for assessing past volcanically forced cooling in the Southern Hemisphere, but the dating and seasonality of the eruptions as well as the continentality and mid-latitude location of the woodland sites may also be important factors for capturing the signal of volcanic cooling.

1 Introduction

Over the last decade, there has been a substantial improvement in tree-ring based millennial-length reconstructions of past summer temperatures across the Northern Hemisphere (Anchukaitis et al., 2017; Guillet et al., 2017; King et al., 2021; Schneider et al., 2015; Stoffel et al., 2015; Wilson et al., 2016). This increase in robustness reflects not only network expansion but also the predominant use of conifer latewood maximum density data (Björklund et al., 2019) that often enables more than 50% of the local/regional instrumental temperature variance to be modelled in regression-based calibrations. Ring-width has been shown to be a particularly poor tree-ring proxy parameter for reconstructing past summer temperatures at inter-annual timescales (Anchukaitis et al., 2012; D'Arrigo et al., 2013; Mann et al., 2012), which can create substantial bias in the assessment of past volcanic forcing.

The importance of common era hemispheric scale paleoclimate reconstructions for the attribution of drivers of past and present temperature change is unquestioned (Hegerl and Zwiers, 2011; Stott et al., 2010). However, there are still uncertainties in these large-scale tree-ring based temperature estimates which are partly related to the tree ring parameters used (Esper et al., 2015; Lücke et al., 2019) and the methods employed to combine these data to create large scale estimates of past climate (Franke et al., 2020). Large volcanic eruptions with stratospheric plumes are one of the most significant external forcing factors that can drive regional and large-scale episodic cooling (Burke et al., 2023; van Dijk et al., 2024a; Fang et al., 2022; Schurer et al., 2014; Toohey et al., 2019) and the new generation of Northern Hemisphere reconstructions has been particularly useful in enhancing our understanding of the impact of volcanic events on past summer temperatures.

Compared to the Northern Hemisphere, the Southern Hemisphere presents a considerable challenge for palaeoclimate research because its much smaller land area greatly limits the availability of terrestrial climate proxy archives. From a dendroclimatic perspective, temperature-limited tree-ring records are largely confined to Tasmania and the mid-latitude regions of New Zealand and South America. Further, despite the well documented importance of utilising maximum latewood density parameters to drive and enhance Northern Hemisphere temperature reconstructions (Briffa et al., 1998; Schneider et al., 2015; Wilson et al., 2016), no single equivalent density record and associated temperature reconstruction exists for the Southern Hemisphere. In fact, as almost all temperature reconstructions developed across the Southern Hemisphere are based on ring-width data, it is perhaps not surprising, therefore, that there is only weak and ambiguous evidence for volcanically forced cooling in this hemisphere (Boninsegna and Hughes, 2001; Higgins et al., 2022; Neukom et

https://doi.org/10.5194/egusphere-2026-4785
Preprint. Discussion started: 28 August 2026

al., 2014; Tejedor et al., 2021). It is paramount that ring density datasets are generated for relevant temperature-sensitive woodland sites in the Southern Hemisphere.

There is a well-known lagged (year T+1) cooling response noted in Northern Hemisphere mid-to-high latitude trees to large-magnitude tropical volcanic events due to the time lag between the eruption and impact of sulphate aerosols in the atmosphere (Esper et al., 2015; Marshall et al., 2021; Wilson et al., 2016). It can be hypothesized that a similar lagged response should exist for the Southern Hemisphere. However, depending on the location and seasonal timing of volcanic eruptions, it is possible that mid-latitude Southern Hemisphere trees could "pick-up" the cooling response before the Northern Hemisphere. Taking Mt. Tambora (eruption April 1815) as an example, this event led to significant cooling in 1816 over northeast north America and western Europe (Luterbacher and Pfister, 2015; Oppenheimer, 2003; Raible et al., 2016). However, there is the potential that temperature-sensitive trees in the Southern Hemisphere could express volcanically forced cooling in the austral summer – 6 months before the cooling expression in the Northern Hemisphere (Figure 1). However, for tropical eruptions later in the year (e.g. Krakatoa – peak eruption August 1883) cooling would likely be expressed in the Northern Hemisphere (boreal summer 1884) before the Southern Hemisphere (austral summer 1884/85). The development, therefore, of temperature sensitive ring density records in the Southern Hemisphere, that potentially could express volcanically forced cooling, will likely provide a more complete dynamical understanding of the timing of the large-scale climate response to high-magnitude explosive volcanic events and potentially help refine dating uncertainties for some events when comparisons are made between both hemispheres (Lücke et al., 2023).

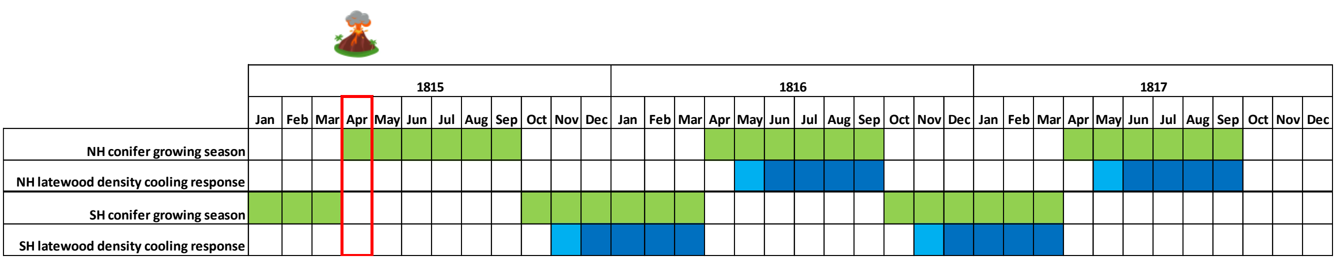

Figure 1. Schematic representation (using the Tambora eruption of April 1815 as an example) of the generalised growing season (green) of conifer trees in the mid-high latitudes of the Northern and Southern Hemispheres (SH) and when ring density (traditional density or blue intensity) data could express a cooling response (blue) to tropical volcanic eruptions. In general, Northern Hemisphere (NH) density records express cooling in the boreal summer (MJJA, JJA or JA) of 1816. The equivalently austral seasonal response for SH conifers will be roughly lagged by six months to the months November to March.

There is a new wave of research assessing novel ways to extract past climatic information from Southern Hemisphere conifer trees. This explorative work, focussing on the three regions of southern Australia, New Zealand and South America, has used Blue Intensity (an image analysis method for attaining relative ring density (Björklund et al., 2024, 2014; Campbell et al., 2007; Rydval et al., 2014)) and quantitative wood anatomical measurements (von Arx et al., 2016; Björklund et al., 2020) to attain temperature calibrations at least as strong as those noted using maximum latewood density data in the Northern

https://doi.org/10.5194/egusphere-2026-4785
Preprint. Discussion started: 28 August 2026

Hemisphere (Allen et al., 2018a; Björklund et al., 2023; Blake et al., 2020; Brookhouse and Graham, 2016; Mundo et al., 2024; O'Connor et al., 2022; Wilson et al., 2021). In South America, stable isotopes have also been the focus of recent dendroclimatic initiatives detailing substantial potential for well calibrated reconstructions of past temperature and hydroclimate (Lavergne et al., 2018; Penchenat et al., 2022). The maturation of this experimental work will substantially enhance our understanding of Southern Hemisphere climate in the coming years.

In this study, we utilise ring-width and Blue Intensity measurements from a network of six near upper tree-line *Araucaria araucana* sites located along a 100 km transect in Northern Patagonia, Argentina to create the first ring-density derived summer surface temperature reconstruction for the region (Figure 2, Table 1). By combining different tree-ring parameters, we develop a January-March austral summer temperature reconstruction with acceptable fidelity back to the early 15th century. This record not only shows that the most recent decade is the warmest for at least the last 600 years, but that there is clear evidence for a regional cooling response to major tropical volcanoes.

https://doi.org/10.5194/egusphere-2026-4785
Preprint. Discussion started: 28 August 2026

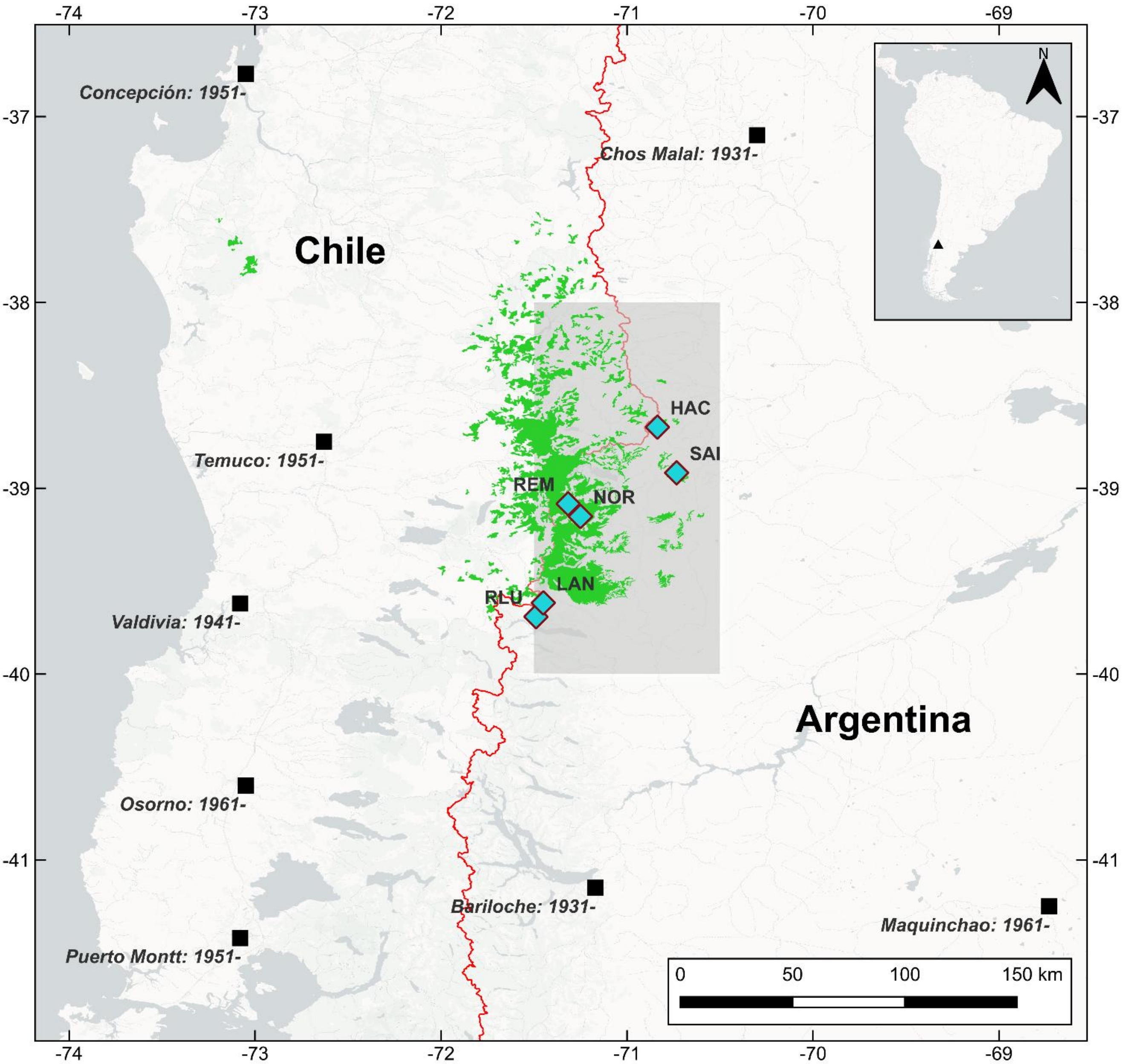

Figure 2: Location map of *Araucaria araucana* sites (light blue diamonds) in relation to the species range (green) and the target CRU TS grid (Harris et al., 2020) (71°30 - 70°30W / 38° - 40° S – grey box) used for analyses. Meteorological stations in the wider region are shown with their start dates. See Table 1 for more tree-ring site details.

https://doi.org/10.5194/egusphere-2026-4785
Preprint. Discussion started: 28 August 2026

2 Methods

2.1 Tree-ring network, parameter measurement and chronology development

Previous dendrochronological studies using ring-width (RW) of *Araucaria araucana* in Argentina identified a mixed influence of previous year's summer temperature (inverse) and current year hydroclimate (positive) on ring-width variability (Mundo et al., 2012). Recent explorative work (Mundo et al., 2024), using Blue Intensity (BI) parameters, identified latewood BI (LWBI) and delta BI (DBI) to express a strong positive correlation with late summer temperatures, while earlywood BI (EWBI) expressed a strong positive (negative) correlation with spring/early summer temperatures (precipitation).

Site Name	Site Code	Latitude	Longitude	Elevation (m a.s.l.)	Chronology Length	No. of Series (trees)	MSL
Pino Hachado	HAC	38°40'22.21"S	70°50'16.11"W	1650 - 1690	1300-2017	85 (46)	333
Sainuco	SAI	38°54'58.60"S	70°44'12.00"W	1660 - 1690	1343-2017	109 (49)	310
Remeco	REM	39° 5'24.02"S	71°19'6.93"W	1320 - 1370	1364-2017	100 (51)	319
Ñorquinco	NOR	39° 9'9.50"S	71°15'6.67"W	1130 - 1150	1618-2017	86 (45)	219
Lanín volcano	LAN	39°37'2.80"S	71°26'35.50"W	1580 - 1600	1324-2017	109 (57)	277
Ruculeufu	RLU	39°41'28.50"S	71°29'22.88"W	1360 - 1400	1555-2017	36 (18)	290

Table 1: Chronology site information for the six *Araucaria araucana* sites used in the study (see Fig. 2). MSL = mean sample length in years.

For this study, six *Araucaria araucana* woodland sites were targeted for new tree coring along a ~100km transect of the southern to mid-range of the species in Argentina (Figure 2). The site elevations range between 1130 and 1690 m a.s.l. (Table 1) which are generally at or close to upper treeline. 2 cores were taken from more than 45 trees at each site, although at one location (RLU) substantially fewer trees were sampled (Table 1). Following standard procedures for BI measurement (Mundo et al., 2024; Rydval et al., 2014), the tree increment cores were stored in slitted straws to allow for sample drying, and in the laboratory were mounted and sanded to a fine polish (up to 1000 grit) so the cells were clearly visible under a microscope. No resin extraction was performed on the cores, as the dark staining for this species (Mundo et al., 2024) is related to fungal discolouration and not resin and could not be removed using standard acetone or ethanol extraction methods. The sanded samples were scanned either at 2400 or 3200 dpi using an Epson V850 scanner calibrated to an IT8.7/2 colour card in conjunction with the SilverFast scanning software. Rings were measured and crossdated using the CooRecorder/CDendro software (Maxwell and Larsson, 2021) and dating was validated within and between sites using COFECHA (Holmes, 1983). We initially used standard tree-ring dating protocols for the Southern Hemisphere, following the so-called "Schulman shift" convention (Schulman, 1956), where a ring is assigned a calendar date to the year in which growth started. Finally, as is the norm for measuring BI and density parameters from Northern Hemisphere conifers (Wilson

https://doi.org/10.5194/egusphere-2026-4785
Preprint. Discussion started: 28 August 2026

et al., 2017), the final ring was not measured to minimise the potential dark/dense ring colouration bias that is often noted due to the ring's proximity to the cambium.

Once the ring boundaries were marked and the samples crossdated, BI parameters were generated using CooRecorder (Buckley et al., 2018; Heeter et al., 2022; Rydval et al., 2014). The BI generation "window" was set to roughly equate to two thirds width of the 5mm sample (160-220 pixels) while the window depth settings set to encompass either the latewood (LW) or earlywood (EW) for each ring. For latewood, the mean reflectance values were taken from the lowest 15% of the darkest pixels, while for earlywood, the mean of the brightest 85% of the pixels was used. As the *Araucaria araucana* latewood blue reflectance data appear to express similar climate response properties to Northern Hemisphere conifers species, the raw EW and LW blue reflectance data were inverted (Rydval et al., 2014) to ensure they correlated positively with their density counterparts allowing the use of the '2024 BI standardised terminology' of LWBI and EWBI (Björklund et al., 2024).

Distinct fungal discolouration is noted in the *Araucaria araucana* samples towards the centre of the tree cores, which imposes a substantial non-climatic-related trend colour-bias in the non-detrended BI data. This transition from dark staining to "clean" wood is generally expressed as a transitional change, although some sharp transitions may also occur for some individual samples (Mundo et al., 2024). When the BI data from all 6 sites are pooled together as cambial age-aligned mean curves (Figures A1A), the average fungal discolouration is generally expressed in the EWBI and LWBI data as a negative exponential curve of gradual transitional change from high BI values (inversion of low reflectance values of the darker wood (Rydval et al., 2014)) in the juvenile years which stabilise after ~250 years in the EWBI data, but with a continued slight decline for LWBI. These long-term non-climatic trends also dominate in the calendar-dated, non-detrended EWBI and LWBI mean chronologies (Figure A1B). As this colour bias is, on average, gradational in nature, such trends can be removed through standard data adaptive detrending methods (Cook et al., 1990; Melvin et al., 2007) as would be used for ring-width (RW) or density data (Figure A1A).

As the colour change is common to both the earlywood and latewood, the potential reflectance bias can theoretically be minimised by creating a delta parameter (Björklund et al., 2014) by subtracting the EWBI data from the LWBI data (hereafter referred to DBI). Theoretically, DBI should correct for common colour change biases between heartwood and sapwood. To date, DBI has been utilized successfully in only a few studies (Björklund et al., 2014; Blake et al., 2020; Fuentes et al., 2018; Reid and Wilson, 2020; Wang et al., 2020; Wilson et al., 2017). Mundo et al., (2024) showed a significant summer temperature response in DBI for *Araucaria araucana*. Although the DBI cambial age aligned curve still portrays a distinct age-related trend (initial 100 year increasing trend following by a decreasing trend (Figures A1A)), the strong age-related trends noted in the raw non-detrended regional composite chronologies of EWBI and LWBI (Figure A1B), are not noted for the DBI data suggesting that the colour bias has been substantially minimised or removed.

https://doi.org/10.5194/egusphere-2026-4785
Preprint. Discussion started: 28 August 2026

Due to the non-linear nature of the cambial-age trends noted in the raw data for each parameter (Figure A1A), detrending was performed using an age-dependent spline (ADS - Melvin et al., (2007)) with a starting spline flexibility of 50-years. This approach allows for the flexible tracking of the initial juvenile years of the different tree-ring parameter series (especially DBI), while allowing for retention of more secular-scale information as the trees become older. As both the EWBI and LWBI express such strong fungal-related colour trend biases (Figure A1A), ADS was implemented to remove both positive and negative long-term trends in the data. For both the RW and DB data, however, the ADS function was constrained to not remove positive trends in the recent period. This approach greatly reduces the removal of any potential warming signal that could be expressed in these data (Heeter et al., 2023; Mundo et al., 2024; Wilson et al., 2019). For each parameter, the final chronology was developed using the "signal-free" (SF) method (Melvin and Briffa, 2008). The SF method allows the retention of the common medium-frequency variability on timescales longer than the mean length of the samples (Table 1) that may be removed by the initial data detrending (Cook et al., 1995).

2.2 Principal component analysis, climate response and reconstruction method

To explore the varying climatic signals expressed by the different tree-ring parameters across the network (Figure 2), principal component analysis (PCA) was performed over a common well replicated period (1701-2017) of the 24 ADS chronologies (four parameter chronologies from the six sites), while correlation response function analysis (CRFA - 1932-2017) was used to assess the temperature response for the individual chronologies, PC scores and regional parameter averages.

Based on the PCA and CRFA results, three calibration experiments were performed to identify an optimal reconstruction method while allowing the extension of the summer temperature reconstruction as far back as possible. Experiment 1 utilised a standard principal component regression approach where PC scores (1701-2017) with an eigenvalue ≥1, derived from the full dataset of 24 parameter chronologies, were used at lags T and T-1 (the latter to model the previous year's relationship with temperature); Experiment 2 used the four-parameter (RW, EWBI, LWBI and DBI) specific PC1 scores (at lags T and T-1), while Experiment 3 utilised regional composite averages of each parameter (at lags T and T-1). The advantage of this latter approach is that a time-varying nesting approach based on changing replication through time (Meko, 1997) could be employed to quantify the decrease in reconstruction quality back in time (see section 3.1).

For each methodological experiment, the TR time-series were shifted forward by 1 year to adjust for the "Schulman shift" (Schulman, 1956). Input data were only considered as potential independent variables if they correlated significantly ($p < 0.05$) with the target temperature season over the 1932-2017 period. Initial split period calibration and validation was performed on the 1932-1974 and 1975-2017 periods (with these periods swapped) to assess stability in the reconstructed signal. A further broad period calibration was performed over 1932-2017 with validation over 1903-1931, a critically

https://doi.org/10.5194/egusphere-2026-4785
Preprint. Discussion started: 28 August 2026

important independent period, as it was not used in the correlation response function analysis or data screening. For each calibration, the subset of series to enter the multiple regression models was determined using the minimum Akaike information criterion (AIC - (Akaike, 1974)). Finally, the reconstruction fidelity was validated using the coefficient of determination (r^2), the reduction of error (RE) and the coefficient of efficiency (CE (Cook et al., 1999)). Final full-period calibration was performed using the 1903-2017 period, while these full-period model residuals were assessed by testing for a linear trend, and 1st order autocorrelation using the Durbin-Watson statistic. Ideally, model residuals should show no linear trend or significant 1st order autocorrelation. Despite the use of the AIC to identify the optimal set of independent variables within the regression models, the variance inflation factor (VIF) was further used to test for multicollinearity between the independent variables within the multiple regression models (Fox, 1997). VIF values < 4.0 denote no significant multicollinearity.

2.3 Climate Models and Simulations

For proxy/model comparison over the target region of study (Figure 2), we used three ensemble last millennium simulations performed with version 1 of the UK Earth System Model (UKESM1), a state-of-the-art model that includes terrestrial and ocean biogeochemistry, an atmosphere-land-ocean-sea ice model, and a comprehensive aerosol and chemistry scheme (Archibald et al., 2020; Sellar et al., 2019). As detailed in (Marshall et al., 2025), two modifications have been made. Firstly, stratospheric volcanic eruptions were simulated using the GloMAP-mode aerosol microphysical scheme (Mann et al., 2010); Secondly, a bug correction was implemented in the aerosol scheme that changes the sulfuric acid vapour as applied in version 1.1 of UKESM (Mulcahy et al., 2023). We further included the CMIP6/ PMIP4 past100 simulations (Jungclaus et al., 2017) of the MPI-ESM1.2-LR (van Dijk et al., 2024b; Mauritsen et al., 2019), the ACCESS-ESM1-5 (Ziehn et al., 2020), the INM.INM-CM4-8 (Volodin et al., 2019), the MIROC-ES2L(Ohgaito et al., 2021a) and the MRI (Yukimoto et al., 2019) models. A brief overview of the models and the simulations can be found in Appendix Table A1. In all PMIP4 models, except the MRI, the volcanic radiative forcing is prescribed with monthly and zonal mean optical parameters calculated with the EVA forcing generator (Toohey et al., 2016) with sulphur emissions from the eVolv2k data set (Toohey and Sigl, 2017). In the MRI model the volcanic forcing is calculated online with the interactive aerosol Model MASINGAR (Yukimoto et al., 2019) and eVolv2k sulphur emissions.

2.4 Superposed Epoch Analysis (SEA)

SEA examines the mean behaviour expressed in a time-series to a series of discrete events (Rao et al., 2019a). SEA was utilised to assess whether there was a significant mean cooling response in the temperature reconstruction to major tropical stratospheric volcanic eruptions. The major tropical eruptions were identified from the eVolv2k database (Toohey and Sigl, 2017) focussing on (1) eruptions located in the tropics, (2) those that expressed high ($> \sim 10$ kg km^{-2}) cumulative sulphur deposition in both Greenland and Antarctica and (3) events that had volcanic stratospheric sulphur injection (VSSI – Tg S) rates at least as high as Mt Pinatubo in 1991 (Table 2). 9 tropical volcanic events were identified (Table 2).

https://doi.org/10.5194/egusphere-2026-4785
Preprint. Discussion started: 28 August 2026

It is possible that there are some minor dating uncertainties with regard to ice core-based estimates of volcanic forcing (Lücke et al., 2023). Even a misdating of only 1 year could weaken any proxy/model comparison when assessing volcanically driven summer cooling. We therefore used slightly different eruption years for assessing the tree-ring based reconstruction and model runs. For the models, as the eruption years are predefined by the volcanic forcing inputs, the dates are prescribed, and we therefore define these as "Model" eruption years (Table 2). For the tree-ring reconstructions, we used a revised eruption dataset which employs several high-time resolution ice-core records from Greenland and Antarctica (see Appendix A1 - "Revised volcanic eruption dates for SEA" and Table A2 for details) to adjust previous dates by considering a mean time lag of 6-7 months between volcanic eruptions and subsequent deposition recorded in the polar ice cores resulting from slow poleward transport of sulphate aerosols in the stratosphere. We consequently adjusted the dating of some unidentified events (e.g. 1808, 1693, 1594 and 1457) within the stated age uncertainties and define these as "Actual" eruption years (Table 2).

Using the identified volcanic eruption years, SEA was performed using the method outlined in Rao et al. (2019a). Multiple SEA tests were performed using all 9 tropical events, and a smaller subset of high magnitude eruptions with SSI values > 15 Tg S and with the inclusion/exclusion of 1457. The SEA was performed by assessing the mean annual value (temperature anomaly or z-score) for all events relative to the mean of the preceding 5 years. Statistical significance was assessed using a random reshuffling method using 10,000 iterations (Rao et al., 2019a). A subsidiary SEA was also performed using the following events, 1808, 1693 and 1457, shifted forward by one year to assess the sensitivity of the SEA results to these minor eruption date adjustments (Table 2).

Volcano Name	Latitude	"Actual" Eruption Year	"Model" Eruption Year	NH flux	SH flux	VSSI
Krakatau	-6.0	1883	1883	17.63	10.40	9.34
Cosigüina	13.0	1835	1835	18.85	9.60	9.48
Tambora	-8.0	1815	1815	38.44	45.80	28.08
Unknown	0.0	1808	1809	32.39	25.40	19.26
Unknown	0.0	1693	1695	24.72	22.50	15.74
Parker	6.1	1640	1641	41.13	14.90	18.68
Huaynaputina	-16.6	1600	1600	38.14	18.70	18.95
Nevado del Ruiz	4.9	1594	1595	11.81	14.80	8.87
Kuwae?	0.0	1457	1458	35.33	63.60	32.98

Table 2: Candidate major tropical volcanic eruptions used for the superposed epoch analysis. These specific eruptions were chosen as they are known to be located in the tropics (25°S – 25°N), express high (> ~10 kg/km2) sulphur flux in both Greenland and Antarctica and have volcanic stratospheric sulphur injection (VSSI – Tg S) rates at least as high as Mt Pinatubo in 1991.

https://doi.org/10.5194/egusphere-2026-4785
Preprint. Discussion started: 28 August 2026

3 Results and Discussions

3.1 Principal component analysis, climate response and reconstruction method

The PCA (1701-2017) of the 24 ADS chronologies identifies 6 principal components with an eigenvalue > 1.0 although most of the variance is explained by the first two eigenvectors (Figure 3A+B). PC1 is dominated by the DBI and RW data with the DBI chronologies loading slightly positively on PC2, while the RW chronologies load slightly negatively on PC2 (Figure 2C). The LWBI and EWBI chronologies dominate PC2 loading positively, but they also express positive (LWBI) and negative (EWBI) loadings on PC1.

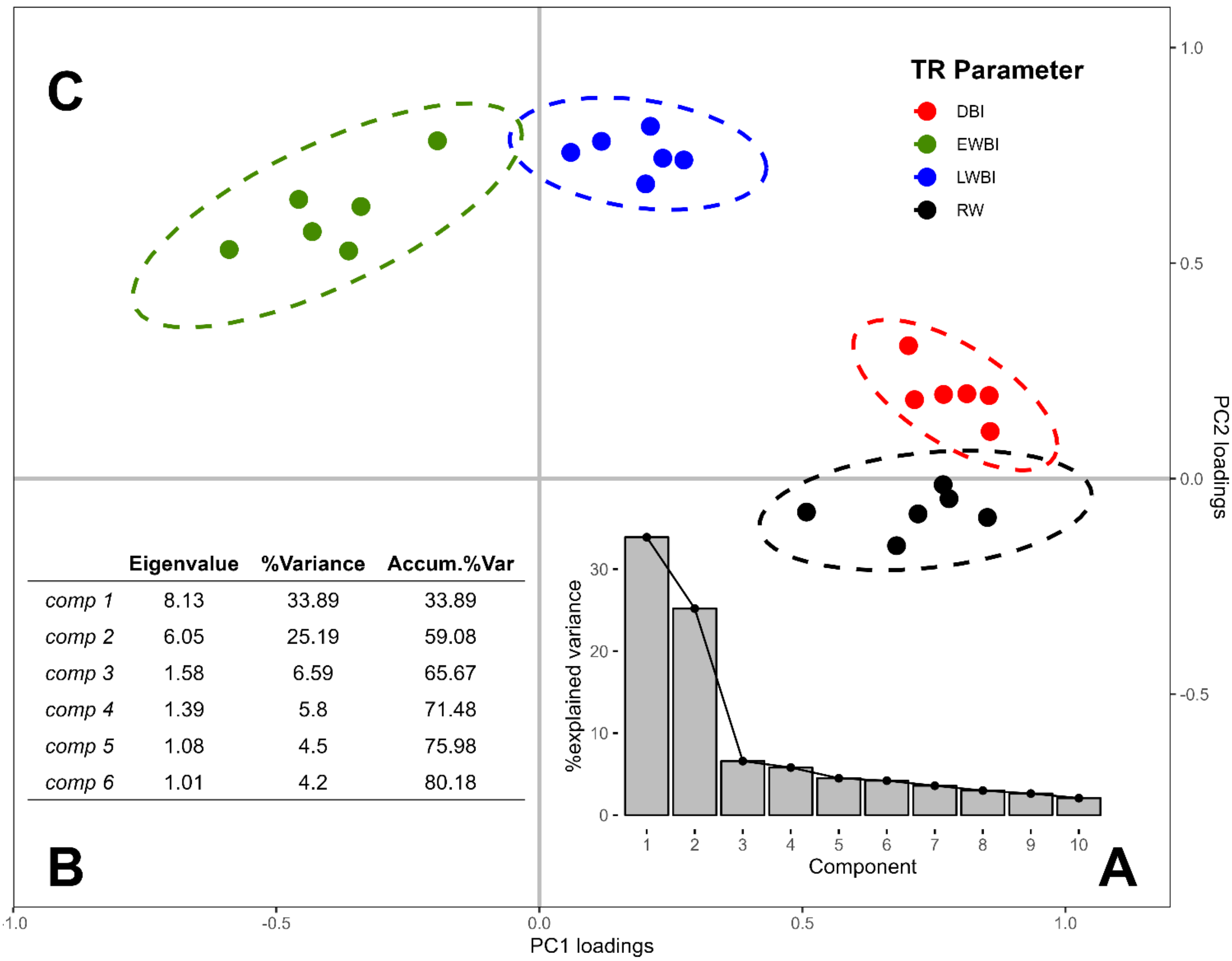

	Eigenvalue	%Variance	Accum.%Var
comp 1	8.13	33.89	33.89
comp 2	6.05	25.19	59.08
comp 3	1.58	6.59	65.67
comp 4	1.39	5.8	71.48
comp 5	1.08	4.5	75.98
comp 6	1.01	4.2	80.18

Figure 3: Principal component analysis (PCA - 1701-2017) using the ADS chronologies for the four parameters from the six sites; A: scree plot of explained variance on each PC; B: PCA results table; C: Scatter plot of loadings of each chronology on PC1 vs PC2 with dots coloured by parameter.

https://doi.org/10.5194/egusphere-2026-4785
Preprint. Discussion started: 28 August 2026

Correlation response functions (1932-2017) between the individual chronologies and monthly mean temperatures (Figure 4A-D) indicates that RW portrays a weak correlation with current year growing summer temperatures, but some sites (SAI, LAN and RLU) show the previously reported (Mundo et al., 2012, 2024) significant inverse correlation with previous summer temperatures. The strongest relationship with temperatures is expressed by both LWBI and DBI, where most sites express significant correlations with December to March temperatures, although the seasonal response for LWBI starts earlier (October) for some sites. Overall, of the BI parameters, the response of EWBI shows the weakest and most inconsistent relationship with monthly temperatures and generally shows a stronger, more consistent inverse correlation with hydroclimate (not shown, but see Mundo et al., (2024)).

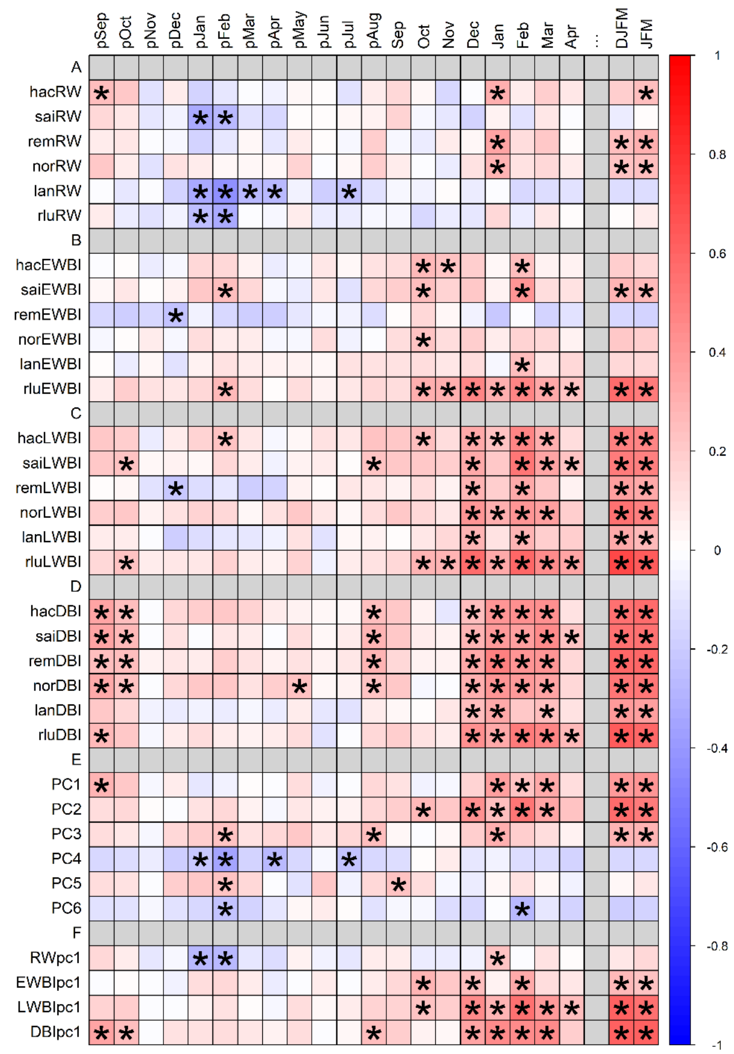

Figure 4: Correlation response function analysis (1932-2017) using CRU TS mean gridded temperatures (Figure 1) with individual site ADS parameter chronologies (A-D), full data-set PC scores (E) as well as parameter specific PC1 (F). * = 95% significance.

https://doi.org/10.5194/egusphere-2026-4785
Preprint. Discussion started: 28 August 2026

The climate responses noted for the individual parameter chronologies are also expressed by the six PC scores (Figure 3B and 4E). However, the PC scores are not represented by consistent loadings by one parameter type. PC1 is a good case in point where the PC score expresses the signal represented by both DB and RW data (Figure 3C). As the climate response of RW is weaker than DB (Figure 4), this impacts the resultant climate signal expressed by PC1. Therefore, a separate PCA was run using the 6 chronologies for each parameter, and the resultant 1st eigenvector scores correlated with mean temperatures (Figure 4F). Focussing on current year summer, the LWBI and DBI PC1 scores correlate similarly with DJFM (0.61 and 0.61) and JFM (0.55 and 0.60) mean temperatures respectively which are stronger than results attained using the traditional full dataset PC1 (0.44 and 0.46) and PC2 (0.55 and 0.49) scores (Figure 4E).

The calibration results for each of the reconstruction method experiments attain strong results with $_{a}r^2$ values generally greater than 0.5 (Table 4). Differences between the approaches become apparent with validation and residual analysis. Standard PC regression (Experiment 1) performs weakest for both JFM and DJFM with poor validation (negative RE and CE values) over the 1975-2017 period despite strong calibration $_{a}r^2$ values over 1932-1975. Further, significant autocorrelation is noted in the full-period model residuals. Calibration and Validation results are much stronger using the parameter specific PC scores (Experiment 2) and regional chronology composites (Experiment 3) although results are marginally weaker when modelling is performed against DJFM temperatures, including negative CE values over the 1903-1931 period and significant residual autocorrelation. JFM therefore provides the best optimal seasonal target for reconstructing past summer temperatures. For all reconstruction options, the variables that entered the models were DBI (Lag T), LWBI (lag T) and RW (Lag T-1). EWBI never entered any of the regression calibration models.

		1932-1974	1975 - 2017			1975 - 2017	1932 - 1974			1932-2017	1903-1931			1903-2017		
	Season	CAL ar2	VAL r2	VAL RE	VAL CE	CAL ar2	VAL r2	VAL RE	VAL CE	CAL ar2	VAL r2	VAL RE	VAL CE	Full CAL ar2	DW	Lin r
Experiment 1	JFM	0.58	0.09	-0.17	-0.71	0.46	0.52	0.60	0.52	0.45	0.59	0.53	0.27	0.48	1.31	0.17
STD PCreg	DJFM	0.56	0.10	-0.54	-1.16	0.27	0.48	0.53	0.43	0.46	0.46	0.57	0.23	0.49	1.02	0.12
Experiment 2	JFM	0.57	0.38	0.56	0.36	0.42	0.56	0.64	0.58	0.54	0.50	0.57	0.34	0.55	1.57	0.13
Parameter PCs	DJFM	0.54	0.28	0.38	0.13	0.53	0.53	0.54	0.45	0.49	0.23	0.33	-0.20	0.46	1.15	0.15
Experiment 3	JFM	0.55	0.38	0.56	0.36	0.38	0.56	0.65	0.54	0.53	0.48	0.48	0.20	0.53	1.56	0.18
Parameter Means	DJFM	0.51	0.26	0.38	0.13	0.51	0.51	0.55	0.46	0.45	0.16	0.33	-0.22	0.42	1.16	0.10

Table 4: Regression-based **calibration and validation experiment results. Experiment 1 utilised the five PC scores (Figure 3) at lags T and T-1; Experiment 2 used the four-parameter specific PC scores (Figure 2A - at lags T and T-1), while Experiment 3 utilises regional composite averages of each parameter (Figure 2A - at lags T and T-1) as the correlation between the parameter PC score and the regional mean chronology was extremely strong (r = 0.99). Calibration and validation performed on the 1932-1974 and 1975-2017 periods (swapped). A further broad period calibration was performed over 1932-2017 with independent validation over 1903-1931. Validation assessment was performed using the square of the Pearson's correlation coefficient (r^2), the reduction of error (RE) and the coefficient of efficiency (CE - Cook et al., (1999)). Final full period calibration was made over 1903-2017 with assessment of the residuals being made by testing for a linear trend, and 1st order autocorrelation using the Durbin-Watson statistic.**

Despite the marginally better calibration/validation results using parameter-specific PC scores (Experiment 2, Table 4), the final reconstruction was developed using the regional composite parameter chronologies (Experiment 3) as (1), the

https://doi.org/10.5194/egusphere-2026-4785
Preprint. Discussion started: 28 August 2026

parameter PC scores and the regional composite averages are strongly correlated (r = 0.99, Figure A2), and (2) using the composite averages allows a nested sub-setting of the tree-ring series to model the change in explained variance and uncertainty back in time as replication decreases (Meko, 1997). Subset nests of the regional records were created using all series that cover the periods from 2017 back to 1875 (n = 374), 1850 (n = 349), 1800 (n = 292), 1750 (n = 204), 1700 (n = 129), 1675 (n = 100), 1650 (n = 82), 1600 (n = 50), 1575 (n = 39), 1550 (n = 26), 1500 (n = 15), 1450 (n = 12) and 1400 (n = 7). For each subset, chronologies were generated for each parameter and separate multiple regression calibrations (using DBI (Lag T+0), LWBI (Lag T+0) and RW (Lag T-1)) performed for each nested variant. To quantify the full range of uncertainty, the standard error (SE) of the regression estimate was calculated for each nest using multiple calibration periods 1902-1931, 1932-1974, 1975-2017 and 1902-2017. A simple inverse model (Y = b0 + (b1 / n) was then used between the number of series (n) in each nest and the SE estimates for each period calibration (Figure A3A) to allow the prediction of how SE changes as a function of replication (n) change through time (Figures A3B+D). Similar nested modelling was also employed to model the change in $_ar^2$, RE and CE through time. For $_ar^2$, the full period calibration period (1903-2017) was used, while for RE and CE validation, calibration was made over the 1932-2017 period, and 1902-1931 used for deriving the validation metrics (Figure A3C+E).

3.2 The Northern Patagonia (NPAT) Summer temperature reconstruction

The *Araucaria araucana* based summer temperature reconstruction for northern Patagonia (hereafter referred to as NPAT) linearly combines regional composite parameter chronologies of ring-width (RW at lag T+1), latewood blue intensity (LWBI, lag T+0) and Delta Blue Intensity (DBI, lag T+0) regional chronologies (Figure A2) and spans the period 1382 – 2017 CE (Figure 5C). Over the 1903-2017 period, NPAT calibrates strongly ($_ar^2$ = 0.53, Figure 5A, Table 4) with mean January-March (JFM) CRU TS 4.05 gridded temperatures (Harris et al., 2020 - Figure 2). The variance inflation factor values for each independent variable (Figure 5C) indicate, despite the similar summer temperature response of LWBI and DBI (Figure 4), there is no significant multicollinearity between the variables, indicating no calibration $_ar^2$ value inflation. For the most recent replicated period, positive reduction of error (RE) and the coefficient of efficiency (CE - Cook et al., 1999) values based on multiple calibration and validation periods indicate a highly skilful reconstruction (Table 4). Correlations of NPAT with the spatial field of JFM mean temperatures (Figure 6A + 6B) indicates that the reconstruction represents summer land temperatures for a large region of South America from 75-65°W / 37-48°S as well as southeastern Pacific sea surface temperatures for these latitudes back to 1850 CE (Figure 6C). Despite the weak common signal of the BI parameters (Figure A4A) and weak expressed population signal strength (Wigley et al., 1984) of the input TR variable chronologies prior to 1550 CE, especially for LWBI and DBI (Figure A4), modelling of the full period calibration $_ar^2$ values (Figure A3C and A3E) suggests that the explained variance remains above 50% back to the mid-17th century (no. of TR series = ~150), drops below 40% around 1500 CE (no. of TR series = ~50) and finally drops below 30% around 1425 CE (n. of TR series = ~20). RE values remain positive back to the late 14th century while CE drops below zero around the 1530s.

https://doi.org/10.5194/egusphere-2026-4785
Preprint. Discussion started: 28 August 2026

The reconstruction therefore should be treated more cautiously prior to the 1530s but still shows some fidelity back to the early 15th century (Figure A3E).

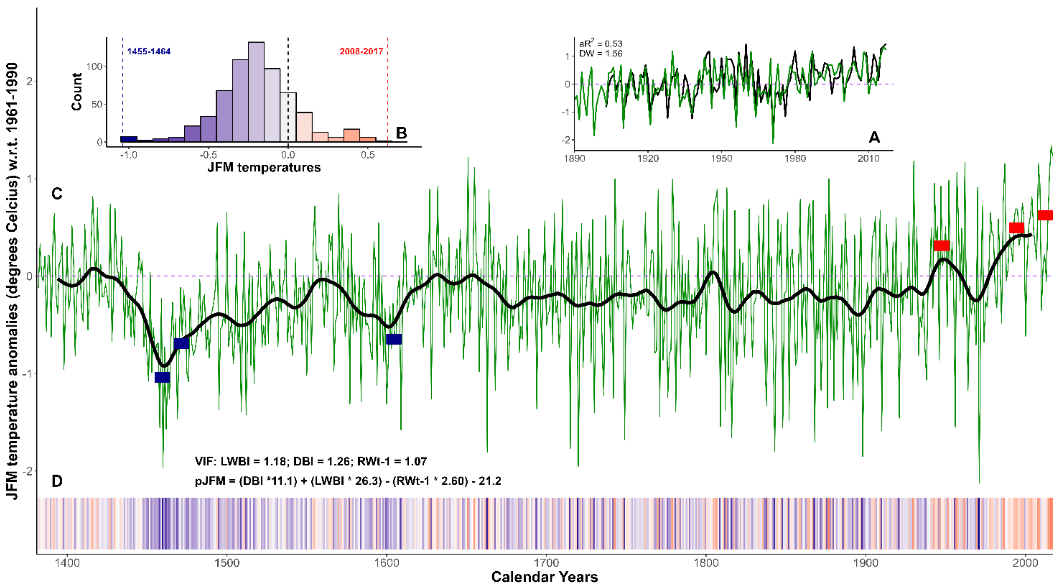

Figure 5: A: Full period scaled (Esper et al., 2005) calibration (1903-2017) with CRU TS mean JFM temperatures (black). Reconstructed values in green. See Table 4 and Figure A3 for full regressed calibration/validation statistics. All values expressed as temperature anomalies with respect to 1961-1990; B: Histogram of decadal mean values with the warmest and coldest decades (see Table 5) highlighted with dashed lines; C: Full period northern Patagonia (NPAT) reconstruction with three none-overlapping warmest (red bars) and coldest (blue bars) decadal periods highlighted (see Table 5). The smoothing line is a 25-year Gaussian filter; D: Climate stripe representation of the full NPAT reconstruction using the colour **scheme of B.**

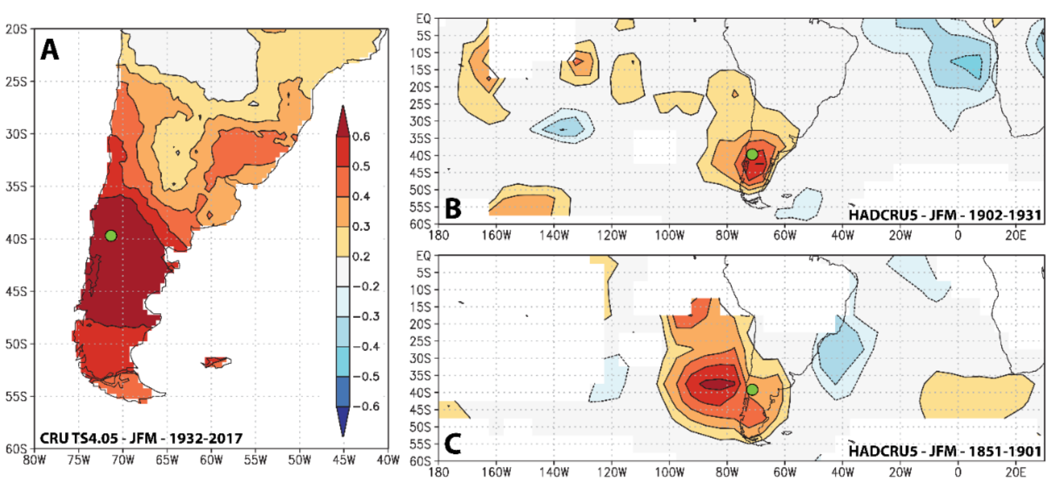

Figure 6: Spatial correlations between the NPAT JFM temperature reconstruction and CRUTS land temperatures (1932-2017 - A) and HADCRU5 land/sea for the periods 1902-1931 (B) and 1851-1901 (C). The study region is denoted by the green-filled circle.

https://doi.org/10.5194/egusphere-2026-4785
Preprint. Discussion started: 28 August 2026

NPAT indicates that the recent period is warmer than any other period of the last 600 years (Figure 5C). The three warmest decades in the NPAT reconstruction are within the last 80 years (Table 5) with the most recent decade (2008-2017) being the warmest on record (0.63 ºC with respect to the 1961-1990 mean, Figure 5B). Of the three coldest decades, 1455-1464 is noteworthy, being 1.04 ºC cooler than the climate norm and coincides with one of the largest volcanic stratospheric sulphur injection events of the last millennium (Toohey and Sigl, 2017) which reflects a potential double eruption event of the tropical Kuwae volcano in Vanuatu as well as a mid-high latitude eruption of the Reclus volcano in southern Patagonia, Chile (Ro et al., 2025). Despite the greater uncertainty of the 15th century estimates, ~35% of the temperature variance is still explained around this cool period of the 1450s (Figure A3). The reconstructed temperature estimates then increase, with some decadal variability, for about a century before dipping again around 1600. A rise to mean climate norm levels is noted around the 1620s-40s followed by a prolonged below norm cooler period (~ -0.3ºC) until the early 20th century when current warming starts. Despite the last 80 years expressing some of the warmest conditions since the early 15th century, the coldest reconstructed year, which agrees well with the instrumental data (Figure 5A), is 1971 (-2.13 ºC), which is then followed by 1460 (-1.96 ºC – Table 6). The ability of the reconstruction to capture both the warmest and coldest extreme years in the calibration period, while also tracking the mid-to-long frequency trends (Figure 5A), indicates that the reconstruction captures interannual to centennial-scale variability very well.

Start	End	Warmest	Start	End	Coldest
2008	**2017**	0.63	**1455**	**1464**	-1.04
1990	**1999**	0.50	**1467**	**1476**	-0.69
1943	**1952**	0.31	**1600**	**1609**	-0.65

Table 5: Three warmest and coldest non-overlapping decades in the NPAT reconstruction

Years	Warmest	Years	Coldest
2016	1.34	**1971**	-2.13
1877	1.30	**1460**	-1.96
2017	1.23	**1720**	-1.95
1651	1.22	**1898**	-1.85
1930	1.18	**1663**	-1.80
1962	1.17	**1843**	-1.80
2008	1.16	**1715**	-1.77
1987	1.15	**1868**	-1.70
1743	1.15	**1749**	-1.68
1655	1.12	**1816**	-1.66

Table 6: The 10 warmest and coldest austral summer (JFM) years in the NPAT reconstruction

https://doi.org/10.5194/egusphere-2026-4785
Preprint. Discussion started: 28 August 2026

Comparison of the NPAT reconstruction with other near independent regional summer temperature reconstructions for South America (Figure 7) indicates substantial differences between the records. Although all records express a warming trend from the mid-20th century, there are marked differences in multi-decadal warmer and colder periods over the last 600 years. For example, NPAT, Lavergne et al., (2018 - hereafter LAV18) and Neukom et al., (2011 - hereafter NEUK11) express cool conditions over the 1850s-1930s while the Lara et al., (2020 - hereafter LAR20) reconstruction suggests warm conditions. While both LAR20 and NEUK11 express warm conditions in the 18th century, NPAT suggests below-average temperatures. Finally, the 15th century extreme cooling expressed in NPAT is only partly mirrored by NEUK11 although the specific timing of maximal cooling is different. LAR20 reconstructs significantly warmer conditions in the 1460-70 period. Running 51-year Spearman's correlations (Figure 8) between each of the four proxy records further highlights the lack of coherence between the different reconstructions even though they all theoretically express a similar austral summer temperature season (note that instrumental DJF and JFM mean temperatures are strongly correlated at 0.84). The only significant and reasonably time-stable correlation (mean $r = 0.58$, $p < 0.01$) is noted between NPAT and LAV18 which provides mutual high frequency validation of both records back to the early 19th century. The LAV18 DJF reconstruction is based on stable carbon isotopes measured from *Fitzroya cupressoides* tree-ring samples from two woodland sites about 200 kms south of the NPAT region. Spatial 1st differenced correlations of the four reconstructions for the 1902-1930 period (Figure A5) – independent of the different study calibration periods - further validates the consistency of the NPAT and LAV18 reconstructions for essentially the same region expressed over their calibration periods (Figure 7). The spatial correlations of LAR20 are generally weak, focussed on the southern tip of South America, while NEUK11 expresses strong correlations but for a region further north of the NPAT study region (~35ºS – 25ºS). It should be noted, however, that NEUK11 is not entirely independent of NPAT and LAR20, as both *Araucaria araucana* and *Fitzroya cupressoides* TR data were included in the input dataset of the NEUK11 study. As NPAT and LAV18 express the summer temperature variability of a similar region of South America (Figures 7 and A5), it is perhaps not surprising that they correlate well with each other (Figure 8) and the lack of coherence with LAR20 and NEUK11 must partly be related to these records expressing the temperature variance for different regions in South America where it is well known that there are strong spatial differences in climate – for example differences in temperature trends between Chilean coastal stations and stations located to the east of the Andes divide in Argentina (Falvey and Garreaud, 2009).

https://doi.org/10.5194/egusphere-2026-4785
Preprint. Discussion started: 28 August 2026

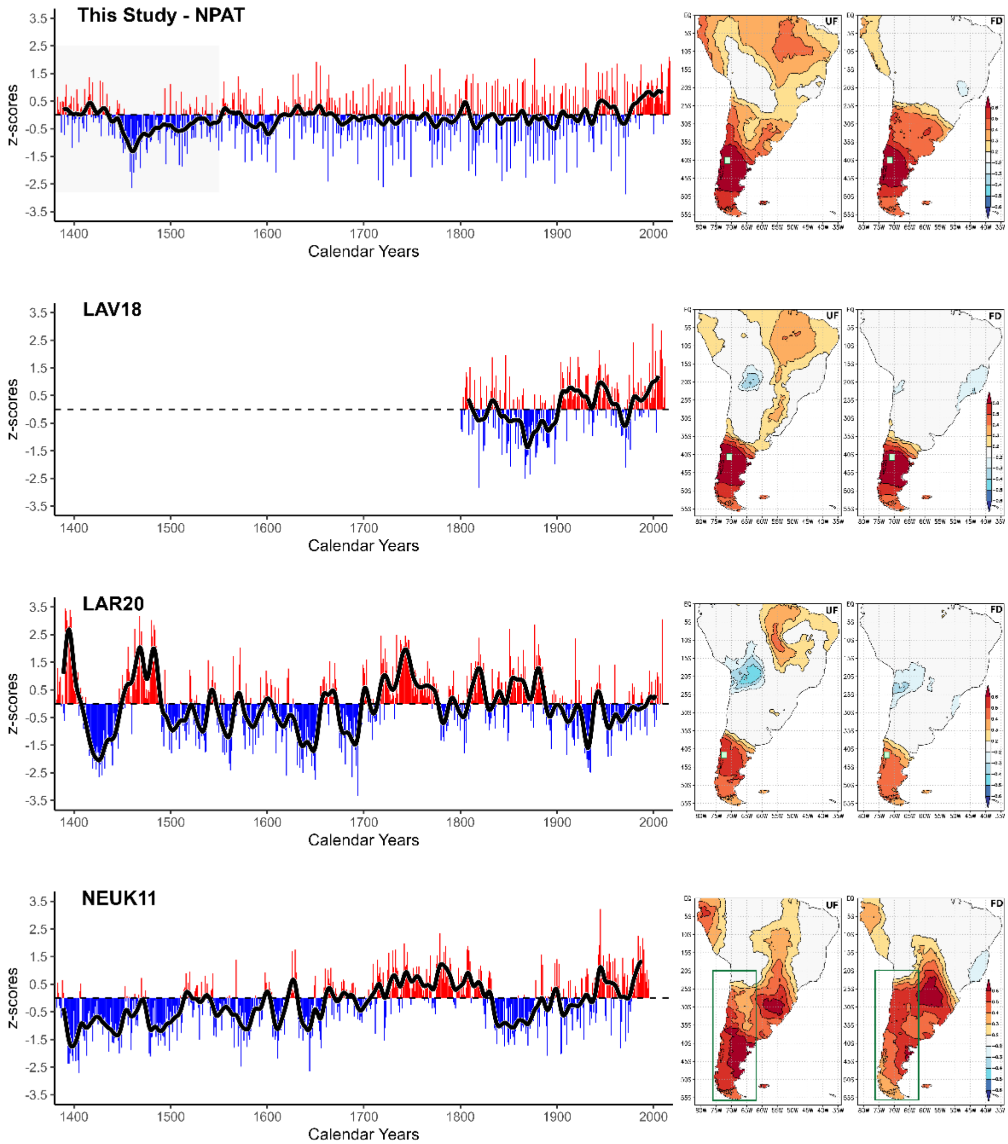

Figure 7: Comparison of the NPAT reconstruction with summer temperature reconstructions from southern South America. LAV18 (Lavergne et al., 2018) based on δ13C data from two sites of *Fitzroya cupressoides*. LAR20 (Lara et al., 2020) is based on ring-width data from eight *Fitzroya cupressoides* sites from Northern Patagonia in Chile. Both LAV18 and LAR20 are geographically located closely to the NPAT study region. NEUK11 (Neukom et al., 2011) is a multi-proxy reconstruction derived from tree ring-width chronologies, ice cores, marine, sediments, corals, documentary records and long instrumental records for a wider region of southern South America. The time-series were normalised to z-scores relative to the mean and standard deviation of the common 1800-1995 period, plotted to highlight positive (red) and negative (blue) anomalies and smoothed with a 15-year Gaussian smoother. The spatial correlation plots for each record utilise the original calibration period and target summer season for each record; NPAT: 1932-2017 JFM, LAV18: 1931–2012 DJF; LAR20: 1959-2009 DJF and NEUK11: 1931-1995 DJF. The grey box for NPAT denotes the period of increased uncertainty due to lower tree replication and associated weaker signal strength (Figures A1B, A2 and A3).

https://doi.org/10.5194/egusphere-2026-4785
Preprint. Discussion started: 28 August 2026

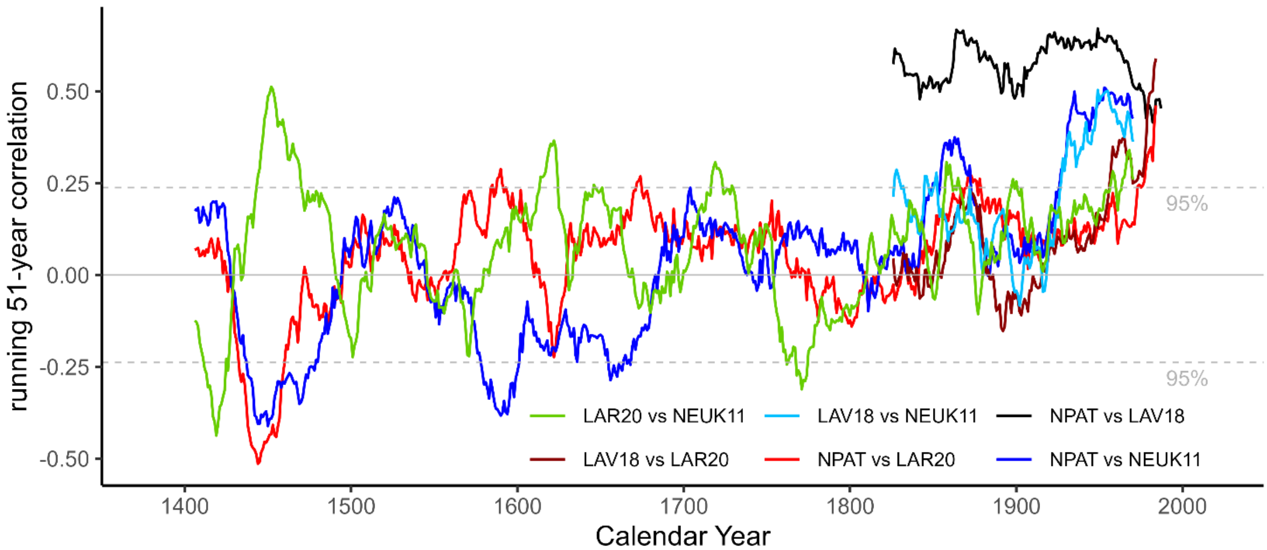

Figure 8: Running 51-year Spearman's rank correlations between each of the four-summer temperature reconstructions presented in Figure 7.

3.3 Volcanic surface cooling response

3.3.1 Southern Hemisphere Tree-ring reconstructions

The standout cold period in the NPAT reconstruction is the late 1450s, with 1460 being the 2nd coldest reconstructed summer and 1455-1464 the coldest decade (Figure 5, Tables 4 and 5). The temporal proximity to one of the largest tropical eruptions (1457/58, Table 2) of the last millennium as well as a concurrent Southern Hemisphere mid-latitude event (Ro et al., 2025) is intriguing. NPAT shows coincident (year T or T+1) cold years (Figure 9 – upper) with many of the large tropical volcanic eruptions of the last 600 years (Tables 2 and A2). Superposed epoch analysis (SEA) of NPAT using these nine eruptions (see Appendix "Revised volcanic eruption dates for SEA") shows a significant (95% C.L.) mean cooling at T+1 of ~0.5 ºC. This weakens slightly with the exclusion of 1457 (Figure 9 – lower).

We hypothesize that if any volcanic cooling response can be seen in the NPAT reconstruction, it should be most strongly driven by the larger-magnitude tropical events. Focussing on the six largest events with > 15 Tg S SSI (1815, 1808, 1693, 1640, 1600, 1457) the SEA does indeed identify a stronger mean cooling of ~1 ºC - with or without 1457. This is the first time that such significant cooling, coincident with major tropical eruptions, has been identified in the Southern Hemisphere, although this result is sensitive to the defined year of the eruption. Further, this volcanic response is expressed in each of the individual tree-ring parameters used to drive the NPAT reconstruction (Figure A6) where both LWBI and DBI express negative (~-1 STDEV) values in year T+0 while RW expresses a positive anomaly in year T+1 which is consistent with the modelled previous year inverse relationship between RW and summer temperatures (Figure 4, Mundo et al., 2012).

https://doi.org/10.5194/egusphere-2026-4785
Preprint. Discussion started: 28 August 2026

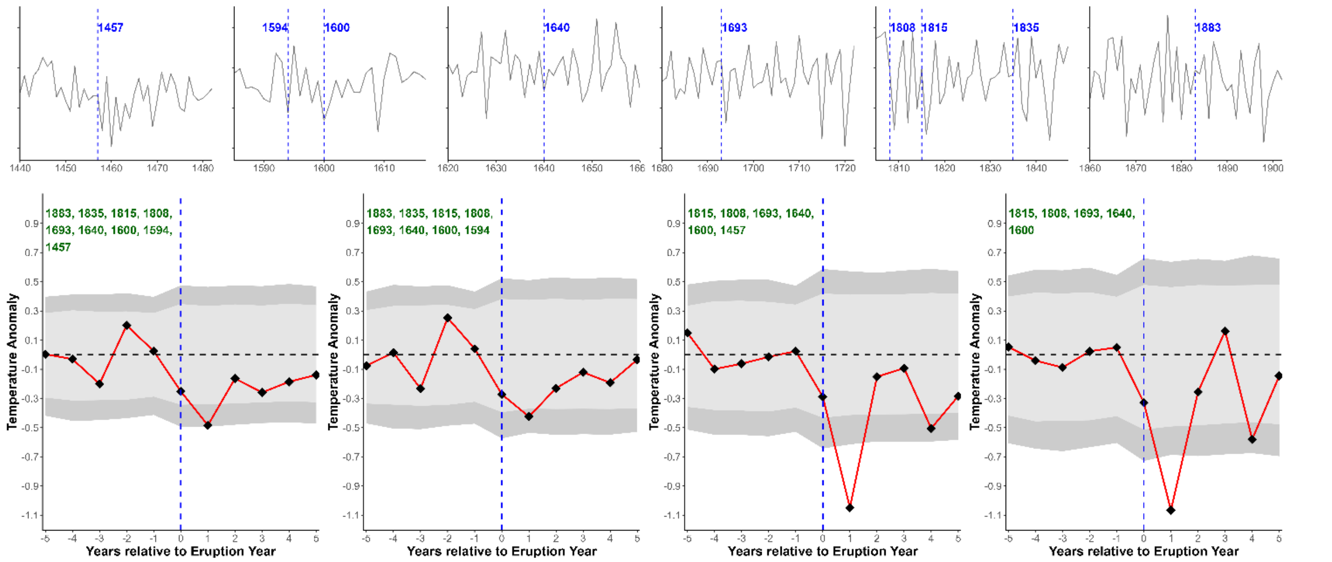

Figure 9: Upper row: Select reconstruction time-series slices (from Figure 5) compared to 9 significant tropical eruption events (Table 2); Lower row: Superposed Epoch Analysis of subset events. The two figures on left use all 9 events with/without 1457 while the two figures on the right use those events with > 15 Tg S SSI – with/without 1457. The outer edges of the light (dark) grey bands denote 95% (99%) confidence ranges.

To date, there has been only weak and ambiguous observational evidence for volcanically forced cooling in the Southern Hemisphere (Boninsegna and Hughes, 2001; Higgins et al., 2022; Neukom et al., 2014; Tejedor et al., 2021). SEA, performed on other tree-ring based summer temperature reconstructions from New Zealand (Higgins et al., 2022), Tasmania (Allen et al., 2018b) and Southern America (Lara et al., 2020; Neukom et al., 2011) using the same six major volcanic events (Figure 10A) shows that none of these records express a mean significant cooling response to these major volcanic events. This result is particularly surprising using the Higgins et al., (2022) record as this was specifically developed to capture volcanically forced cooling in New Zealand. Overall, as most of these SH reconstructions utilised RW data only, this result is perhaps not surprising as RW generally expresses a weak or dampened volcanic response in Northern Hemisphere tree-ring records (Anchukaitis et al., 2012; Wilson et al., 2016). However, the fact that the NPAT RW data do show a positive response (T+1, Figure A6) to major volcanic events highlights that the assumption that RW is a poor proxy for studying past volcanic influences on growth (Anchukaitis et al., 2012) may not always hold for different species, especially if they express a complex response to climate (Figure 4).

The weak volcanic response in other regions of the Southern Hemisphere, however, may not just be related to the overall reliance on RW. Allen et al. (2018b), using a range of quantitative wood anatomical parameters, as well as RW, developed an ensemble of summer temperature reconstructions for Tasmania explaining 59-64% of the temperature variance. As shown in Figure 10A, their record (ALL18) did not identify a significant response to volcanic forcing and Allen et al., (2018b)

https://doi.org/10.5194/egusphere-2026-4785
Preprint. Discussion started: 28 August 2026

hypothesised that this could be related to the dominance of the oceanic signal and its influence on western maritime terrestrial land temperatures. Rydval et al., (2017) derived a similar hypothesis from their maritime influenced Scottish temperature reconstruction which expressed a much weaker response to past major volcanic eruptions compared to the more continental based TR reconstructions from Scandinavia (Esper et al., 2014; Matskovsky and Helama, 2014). Harvey et al., (2020), using historical simulations from the Coupled Model Intercomparison Project (Phase 5), also noted a stronger response to 19th/20th century major eruptions in the austral autumn/winter for the more continental regions of the SH. It is therefore possible that the location of tree-ring records, and the continentality of the sites, is also important for such data to potentially express a volcanic forcing signal. As the *Araucaria araucana* stands sampled for this study are located on the eastern side of the Andes, a region with a more continental dry climate than the wetter western locations of Tasmania (Allen et al., 2018b) and New Zealand (Higgins et al., 2022) this hypothesis might well hold.

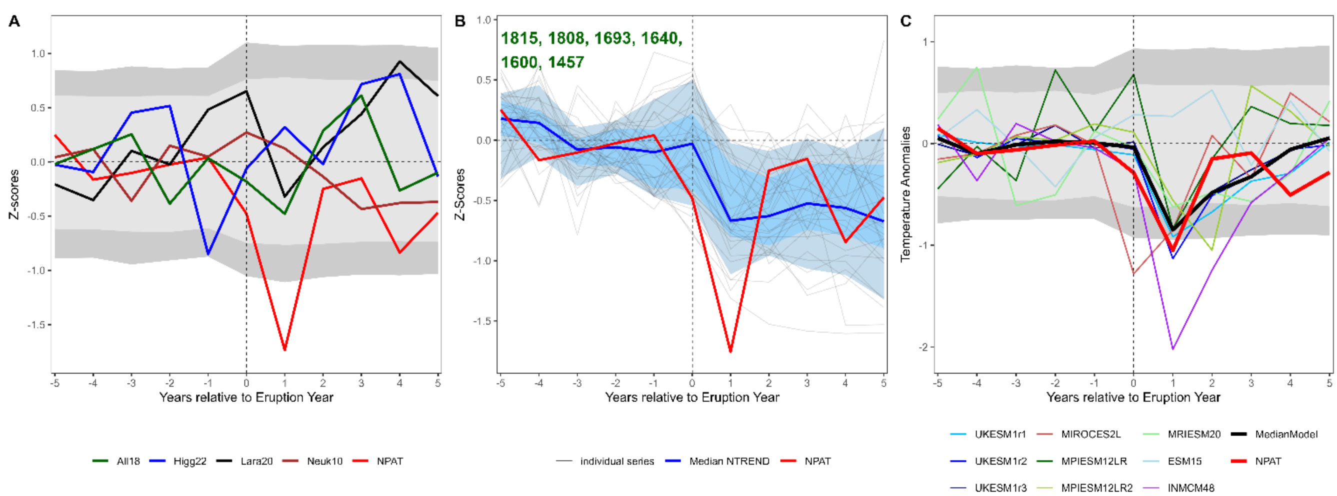

Figure 10: Superposed Epoch Analysis (SEA). A: NPAT reconstruction compared to four summer temperature reconstructions (transformed to z-scores) from Southern America and the wider Southern Hemisphere (Tasmania - Allen et al., (2018b) and New Zealand - Higgins et al., (2022)) focussing on the 6 largest tropical eruptions (1815, 1808, 1693, 1640, 1600, 1457 - Table 2) since 1400 with > 15 Tg S output. The light (dark) grey envelopes denote the 95% (99%) confidence limit for the minimum/maximum error values for each reconstruction SEA; B: Comparison of NPAT with the individual N-TREND TR series for the same "Actual" eruption years as A. All time-series were transformed to z-scores over the 1381-1988 common period. The SEA is performed on individual local TR records that went back prior to 1400 used in the N-TREND Northern Hemisphere temperature reconstruction (Wilson et al., 2016). The blue line is the median of the individual N-TREND series SEA results, while the inner and outer and light blue envelopes denote the 50% and 90% upper/lower percentiles of the N-TREND ensemble. The red line denoted the equivalent SEA results for the NPAT reconstruction. C: NPAT compared to the nine model simulations (Tables 2 and A1), transformed to temperature anomalies over the common 1381-1849 period, using the "Actual" and "Model" eruption years (Table 2) for NPAT and models respectively. The light grey envelope denotes the 99% confidence limit for NPAT SEA while the dark grey envelope denotes the mean 99% confidence limit for the model-based analysis.

https://doi.org/10.5194/egusphere-2026-4785
Preprint. Discussion started: 28 August 2026

3.3.2 Northern Hemisphere Tree-ring reconstructions

To compare NPAT with Northern Hemisphere temperature sensitive tree-ring reconstructions, the 34 longest records that go back to 1382 from the N-TREND dataset (Wilson et al., 2016) and NPAT were normalised to z-scores over their common period and SEA performed on each record using the same 6 major tropical volcanic events (Figure 10B). Although, as expected, the mean response to these tropical eruptions in the individual N-TREND series is at T+1 (Esper et al., 2015; Stoffel et al., 2015; Wilson et al., 2016), not one single N-TREND series shows the magnitude of relative cooling that is expressed in NPAT. The extent of this cooling does not change if the "actual" eruption dates for 1808, 1693 and 1457 are shifted forward by 1 year although the maximal mean cooling response in NPAT shifts to T+0 (see Figure A7) which is incompatible to the 6-7 months transport of aerosols from the tropics to mid-latitudes, suggesting that the assigned "actual" eruption dates (Table 2 and see "Revised volcanic eruption dates for SEA" in the Appendix) are potentially correct.

3.3.3 Climate Models

SEA results comparing NPAT with 9 climate model simulations (using model-based eruption years - see Table 2 and methods) shows a remarkable agreement for most models (Figure 10C). All models express significant cooling at year T+1 except for MIROCES2L and MPI-ESM12LR2 which show maximal cooling at T+0 and T+2 respectively. For the MIROC simulation, the volcanic response is earlier at T+0, which may be related to a different implementation of volcanic forcing (Villamayor et al., 2023), but the amplitude of cooling is also comparable with the NPAT reconstruction. The two MPI-ESM, MRI and UKESM simulations have similar volcanic responses as the NPAT reconstruction, where the temperature anomalies drop between -0.5 and -1 °C. The INMCM48 model expresses the greatest T+1 cooling suggesting that this simulation has a stronger volcanic response. Overall, the model median expresses a very similar response structure with a maximal T+1 cooling of ~0.8 °C, compared to the ~1°C observed for NPAT.

To explore the hypothesis that the location of tree-ring records, and the continentality of the sites (section 3.3.1) might have an influence on the sensitivity of surface temperature to volcanic forcing, we further examined the PMIP4 simulations (Jungclaus et al., 2017), by comparing the NPAT regional model response (Figure 10C) with the regions of New Zealand (47-42° S, 167 – 172 ° E) and Tasmania (43-41 ° S, 145-147 ° E) representing the tree-ring based reconstructions. Overall, the mean volcanic response to the same tropical events (model years 1458, 1600, 1641, 1695, 1809 and 1815 – Table 2, Figure 11A-C) is substantially weaker or even non-existent compared to the NPAT region. Further, using the EVA-Ensemble (Timmreck et al., 2024) for idealised tropical summer (June) eruptions of varying amounts of stratospheric sulphur injection indicates that only the larger tropical eruptions (> 10-20 Tg S) could potentially be expressed in the mid latitudes of the Southern Hemisphere and again, the signal is substantially stronger for the NPAT region compared to New Zealand and Tasmania (Figure 12A-C). This effect can be spatially seen in temperature anomaly maps with the model simulations of varying stratospheric load (Figure 13). The Southern Hemisphere mid-latitudes (40-60° S) show only a weak cooling response. However, a stronger cooling is expressed at latitudes around 25-30° S which increases substantially for larger

https://doi.org/10.5194/egusphere-2026-4785
Preprint. Discussion started: 28 August 2026

magnitude events. South Island New Zealand, at least within this set of simulations, expresses almost no volcanic cooling, even for the very largest magnitude events (Figure 13C, F). These observations are in agreement with Robock and Mao, (1995) who noted, using observational data, significant Southern Hemispheric cooling at lower latitudes (< 30º S) but only weak cooling between 40 and 60 º S. Further, Harvey and Grab, (2022), using CMIP5 models, showed strong mainland Australia cooling for March-May in 1884 after Krakatau, but weaker regional cooling in Tasmania and southern New Zealand. As Allen et al., (2018b) hypothesised, the reduced cooling response at higher southern latitudes is likely related to the increasing influence of the Southern Ocean, where large oceanic heat capacity and mixed-layer buffering dampen the surface temperature response to volcanic radiative forcing. In addition, circulation responses associated with high-latitude Southern Hemisphere variability, including changes in the Southern Annular Mode (SAM, Fogt and Marshall, (2020)), may further modulate regional temperature anomalies by altering meridional heat transport and the strength and position of the Southern Ocean westerlies. Ultimately, the simulations indicate that tropical volcanic cooling is not uniformly distributed across the Southern Hemisphere, but instead exhibits a pronounced meridional gradient with maximal cooling focussed on 25–30°S with substantially weaker cooling poleward of approximately 40°S.

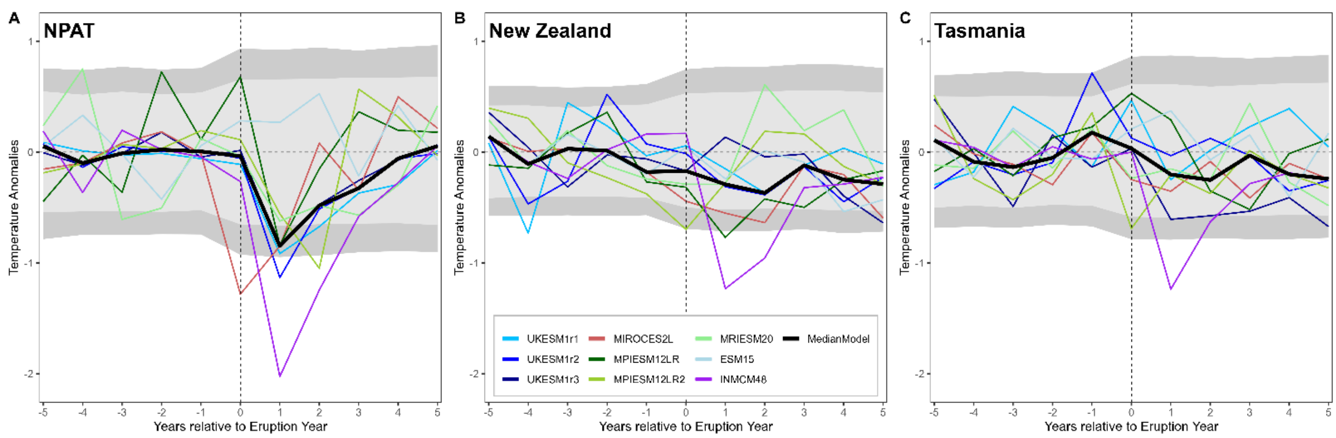

Figure 11: Superposed Epoch Analysis (SEA) of the 9 PMIP4 model simulations for the NPAT region (A – see Figure 10B), New Zealand (47-42 S, 167 – 172 E- panel C) and Tasmania (43-41 S, 145-147 E – panel C) using the "Model" eruption years with > 15 Tg S output (Table 2). The light (dark) grey envelopes denote the 95% (99%) confidence limit for the minimum/maximum error values for each model-based SEA.

https://doi.org/10.5194/egusphere-2026-4785
Preprint. Discussion started: 28 August 2026

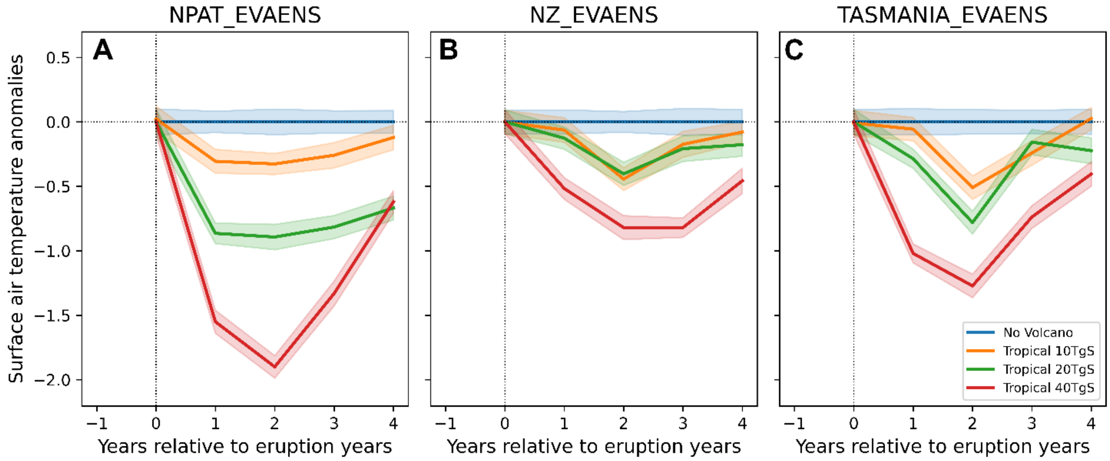

Figure 12: Ensemble mean over 100 members of JFM surface air temperature for the same three regions as Figure ~~S~~11 (A - C) using the EVA-ensemble (Timmreck et al., 2024) of No Volcano ensemble, Tropical summer eruptions with 10, 20, and 40 Tg Sulphur ensemble. The shading is the standard error. The anomalies are calculated from the climatology of the No Volcano ensemble in year 0. Peak cooling is express in year T+2 in the higher stratospheric sulphur injection simulations, as the cumulative cooling is not fully expressed in these regions until the 2nd year – see Figure 1.

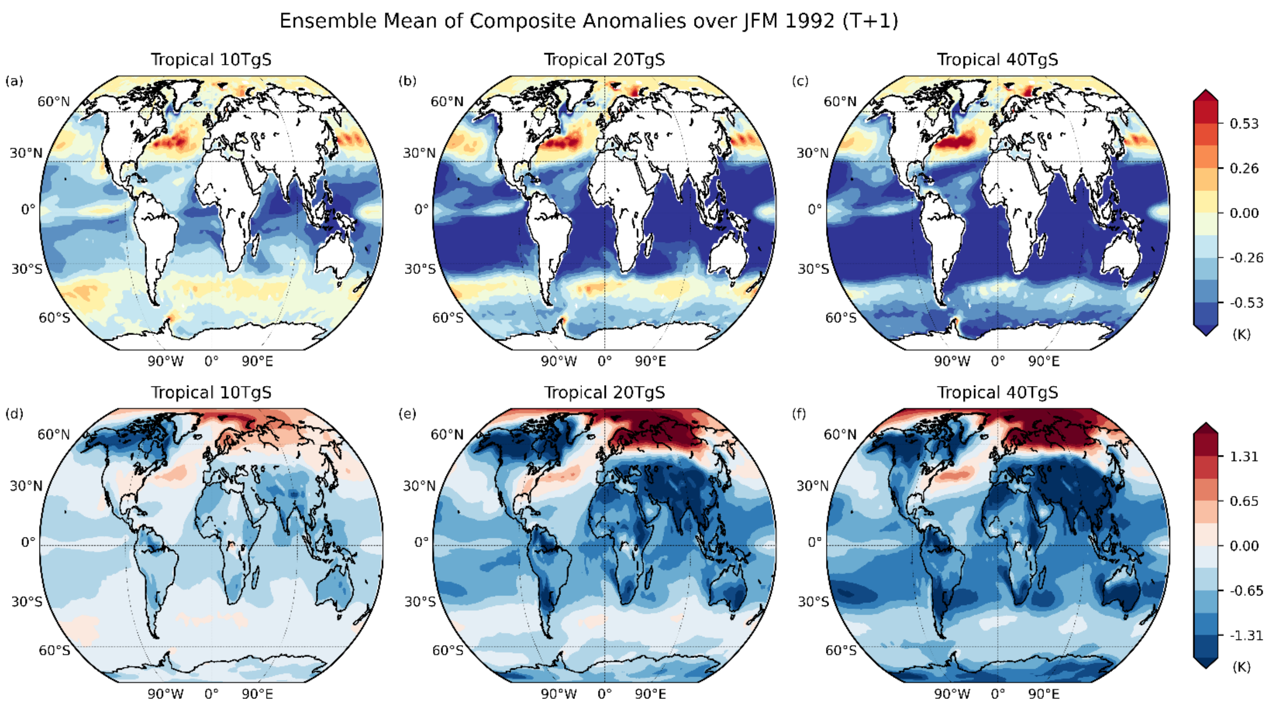

Figure 13: Ensemble mean of JFM sea surface temperature in the year T+1 after an idealised Pinatubo tropical eruption simulation for 10 Tg S (A), for 20 Tg S (B) and for 40 Tg S (C); D-F are for surface air temperature.

4 Conclusions

Despite many decades of dendroclimatic work in the Southern Hemisphere to reconstruct past temperature variability (Boninsegna et al., 2009; Cook et al., 1992, 2000, 2002; Lara et al., 2020; Lara and Villalba, 1993; Villalba, 1994; Villalba et al., 2003), until recently, the only tree-ring parameter used was ring-width (RW). The lack of maximum latewood density (MXD) data, despite its well-known importance for understanding the dynamical response of past summer temperature variability to significant stratospheric volcanic eruptions (Anchukaitis et al., 2012; Briffa et al., 1998), is potentially one of the primary reasons why minimal proxy-based evidence for past volcanic forcing in the Southern Hemisphere has been observed.

Building on recent studies exploring the utility of Blue Intensity (BI) to express strong robust summer temperature signals from Southern Hemisphere conifers (Blake et al., 2020; Mundo et al., 2024; O'Connor et al., 2022; Wilson et al., 2021) we have developed the first relative density BI-dominated summer temperature reconstruction for South America. The reconstruction (NPAT: 1382 – 2017 CE) was developed using regional composite records from six sites of multiple tree-ring parameters (RW, LWBI and DBI), with their linear combination explaining 53% of the January-March temperature variance (Figure 5). NPAT captures the interannual to multi-decadal time-scale information expressed by the instrumental record very well and portrays past mean summer land temperatures for a broad region of southern South American between 37° S and 48° S (Figures 6, 7 and A5). In the context of the past 600 years, the most recent decade (2008-2017) is the warmest on record highlighting the unprecedent nature of recent warming in the region. The coldest decade (1455-1464) coincides with the major Kuwae volcano in Vanuatu (Table 2) as well as a mid-high latitude eruption of the Reclus volcano in southern Patagonia, Chile (Ro et al., 2025), both likely influencing the largest sulphur flux to the Southern Hemisphere for the last 600 years.

Superposed epoch analysis (SEA - Rao et al., 2019b) indicates a strong volcanically forced mean cooling signal at year T+1 in NPAT when compared with major (> ca. 15 Tg S) tropical volcanic eruptions of the past 600 years (Figure 9). Comparison of the NPAT SEA results with a range of historical model simulations (Figure 10C) identifies a similar overall mean cooling response (~0.8-1 ºC) with the models in the year after the volcanic event although one must be cautious with the eruption years of the proxy data as there are minor dating uncertainties with regards to ice core-based estimates of volcanic forcing and the season of the eruptions are often not known (Lücke et al., 2023; Marshall et al., 2024). This is not an issue for the models as the model eruption years are known, but possible slight dating uncertainties in the ice-cores would have an impact of the SEA results for the TR reconstructions. However, the stratigraphic proximity of the few major unidentified eruptions to well dated historic eruptions (e.g. in 1477, 1600, 1667, 1783 and 1815 CE) has strongly reduced uncertainties to a minimum. When the mean SEA response of NPAT is compared with similarly long temperature-sensitive Northern Hemisphere (NH) records from the N-TREND (Wilson et al., 2016) dataset, the relative cooling in NPAT is

https://doi.org/10.5194/egusphere-2026-4785
Preprint. Discussion started: 28 August 2026

substantially greater than most of the individual N-TREND series, although many of the NH records utilised RW data (Figure 10B). This observation strongly indicates that volcanically forced cooling in the SH can at least be on par with observations in the NH for some regions and even adjusting the dates of some key volcanic events (1808, 1693 and 1457) does not change the basic conclusion although the earlier assigned date for these events (Table 2) results in the theoretical T+1 cooling response (Figure 10C vs. Figure A7) as opposed to a T+0 response if these events are shifted forward by 1 year.

The relatively small amount of land in the mid-latitudes of the SH compared to the NH results in a substantially different dynamical situation between the two hemispheres. The NPAT reconstruction clearly shows evidence of a strong response to past major tropical volcanic eruptions and is the first tree-ring based reconstruction in the Southern Hemisphere to show this. Although this is likely partly related to the use of relative wood density parameters (LWBI and DBI) which have been shown, in the Northern Hemisphere, to be superior for capturing a volcanic related cooling response (Anchukaitis et al., 2012), a similarly strongly calibrated record, using quantitative wood anatomical data, from Tasmania (Allen et al., 2018b), did not show any significant strong volcanic response. It is likely therefore, that other factors are at play.

Model simulations, (Figures 13) clearly show a strong meridional cooling response pattern where it is strong at lower latitudes (< 30º S) but is much weaker in the mid-latitudes. The spatial representation of cooling in the EVA-Ensemble (Timmreck et al., 2024) suggests that, of the three mid-latitude regions in South America, southern Australia, and New Zealand where high-elevation temperature-sensitive trees could theoretically record volcanically forced climate variability, northern Patagonia represents the region most likely to preserve a detectable volcanic cooling signal. This appears particularly evident on the drier eastern flank of the Andes, where the influence of maritime conditions is reduced compared with the wetter, oceanically influenced regions of Tasmania and New Zealand. The stronger expression of volcanic cooling in the more continental environment of NPAT suggests that ocean–atmosphere interactions and associated internal climate variability may dampen or obscure the surface temperature response to short-lived external forcing in these regions. In particular, variability associated with large-scale atmospheric modes such as the Southern Annular Mode (SAM; Fogt and Marshall, (2020)) may exert a stronger control on temperature variability in the Southern Hemisphere mid-latitudes, particularly in ocean-dominated regions where the thermal inertia of the surrounding oceans moderates the land-surface response. Conversely, the reduced maritime influence and lower thermal buffering of continental interiors such as northern Patagonia may allow the radiative cooling effects of volcanic eruptions to be more clearly expressed.

Further work is needed to explore these issues. More broadly, across the Southern Hemisphere, it is essential that the dendroclimatic community prioritise the development of ring density, related wood anatomical parameters (von Arx et al., 2016; Björklund et al., 2020, 2014; Rydval et al., 2014, 2024) and stable isotope (Lavergne et al., 2018; Meier et al., 2020) proxy records from additional mid-latitude tree-ring sites. Such data will substantially improve the calibration fidelity of temperature reconstructions relative to RW-only variants and provide more robust estimates of past austral summer

https://doi.org/10.5194/egusphere-2026-4785
Preprint. Discussion started: 28 August 2026

temperatures across these climatically important regions. At the regional scale, a valuable test of the hypotheses proposed here regarding continentality and volcanic cooling would be to extend the *Araucaria araucana* network westwards into the wetter Chilean Andes, enabling direct comparisons across the Andean divide. Such an approach would improve our understanding of the relative influence of large tropical stratospheric eruptions on regional temperature variability in Patagonia.

https://doi.org/10.5194/egusphere-2026-4785
Preprint. Discussion started: 28 August 2026

Appendix A

A.1 Revised volcanic eruption dates for SEA

The exact timing and location of large tropical volcanic eruptions with stratospheric sulphur injection (SSI) exceeding that of the Pinatubo 1991 eruption is only known for a few cases over the past 600 years (Toohey and Sigl, 2017). These include the 1883 eruption of Krakatau (Indonesia), the 1835 eruption of Cosigüina (Nicaragua), the 1815 eruption of Tambora (Indonesia), the 1640-41 winter eruption of Mt. Parker (Philippines) and the 1600 eruption of Huaynaputina (Peru). The exact dates and locations of several other similar large eruptions which have produced major sulphate deposition anomalies over the ice-sheets of Greenland and Antarctica (i.e. in c. 1809, 1694, 1595 and 1458) are however uncertain, and a range of volcanic eruption dates has been proposed on the basis of polar ice-core records (Crowley and Unterman, 2013; Gao et al., 2008; Plummer et al., 2012; Sigl et al., 2013, 2015). This is due to 1) the interpretation of uncertainty in the annual layering of these ice cores and 2) additional uncertainties arising from a poorly constrained time lag between a volcanic eruption in the lower latitudes and the subsequent start of volcanic sulphur deposition on the polar ice sheets linked to aerosol formation and stratospheric transport processes (Marshall et al., 2021). The latter is estimated at around six months using very high snow accumulation ice-core records (i.e. >40 cm water equivalent per year) from Greenland and Antarctica which are well suited to constrain the year and seasonal timing of volcanic sulphur deposition over the polar ice sheets (Marshall et al., 2018).

Here, we compiled high-resolution sulphur and sulphate records from high-snow accumulation (i.e. >20 cm water equivalent per year) ice-core sites in Greenland (D4i(Fang et al., 2023), Summit(Keegan et al., 2014; Stoffel et al., 2022), NEEM-2011-S1(Sigl et al., 2013) and Antarctica (WDC(Sigl et al., 2013), DIV2010(Sigl et al., 2014), DSS(Plummer et al., 2012)) between 1450 and 1900 CE (Table A2). We use these records to evaluate for a reduced eruption dataset which include nine eruptions with VSSI >9 TgS that also produced a major volcanic sulphate deposition anomaly (i.e. >10 kg km^{-2}) in Antarctica where the mean time lag between the known volcanic eruption dates (N=5) and the subsequent start of volcanic sulphur (or sulphate) deposition on the polar ice sheets are well constrained. We excluded the value obtained from the Greenland ice cores following the Mt. Parker eruption which started in late December 1640 and lasted until early January 1641, because a major volcanic eruption of Komaga-take in Japan, starting in summer 1640, may have also contributed to the sulphate deposition in Greenland. We find a time lag of 0.58 ± 0.20 years (1 STDEV, N=4) for Greenland and 0.52 ± 0.17 years (1 STDEV, N=5) for Antarctica, respectively, which we subtract from the mean dates of the volcanic sulphur rise from both ice sheets to estimate the dates of the four unidentified major eruptions discussed above. The projected mean eruption dates for these four eruptions using the ice-core records and estimated lag-times in Greenland are 1809.1, 1694.0, 1594.4, and 1458.8 CE, while those obtained from Antarctica are 1809.0, 1694.4, 1594.6 and 1457.9 CE. Considering that various processes (e.g. snow mixing by wind on the surface, water mixing during analytical analysis) have the potential to slightly broaden the sulphur peaks and thus apparently reduce the actual time lag between an eruption and the subsequent

https://doi.org/10.5194/egusphere-2026-4785
Preprint. Discussion started: 28 August 2026

beginning of polar sulphate deposition we propose that the lower age bound (using the STDEV of the time-lag uncertainties) best represents the true age of the unidentified eruptions. Consequently, we use the refined eruption dates of 1808, 1693, 1594 and 1457 CE with an associated uncertainty of +1 ±1 year (see Tables A2 and 2). An eruption late in 1808 has previously been proposed based on observations of an atmospheric dust veil in South America (Guevara-Murua et al., 2014). The eruption dates suggested previously (1809, 1695, 1595 and 1458 CE) for these events form the basis of the recommended PMIP4 forcing (Jungclaus et al., 2017; Toohey and Sigl, 2017) are within error and are therefore not statistically different from our revised dates but are consistently younger since no time-lag in deposition had been considered. We also provide SEA results using these later-date options (Figure A7).

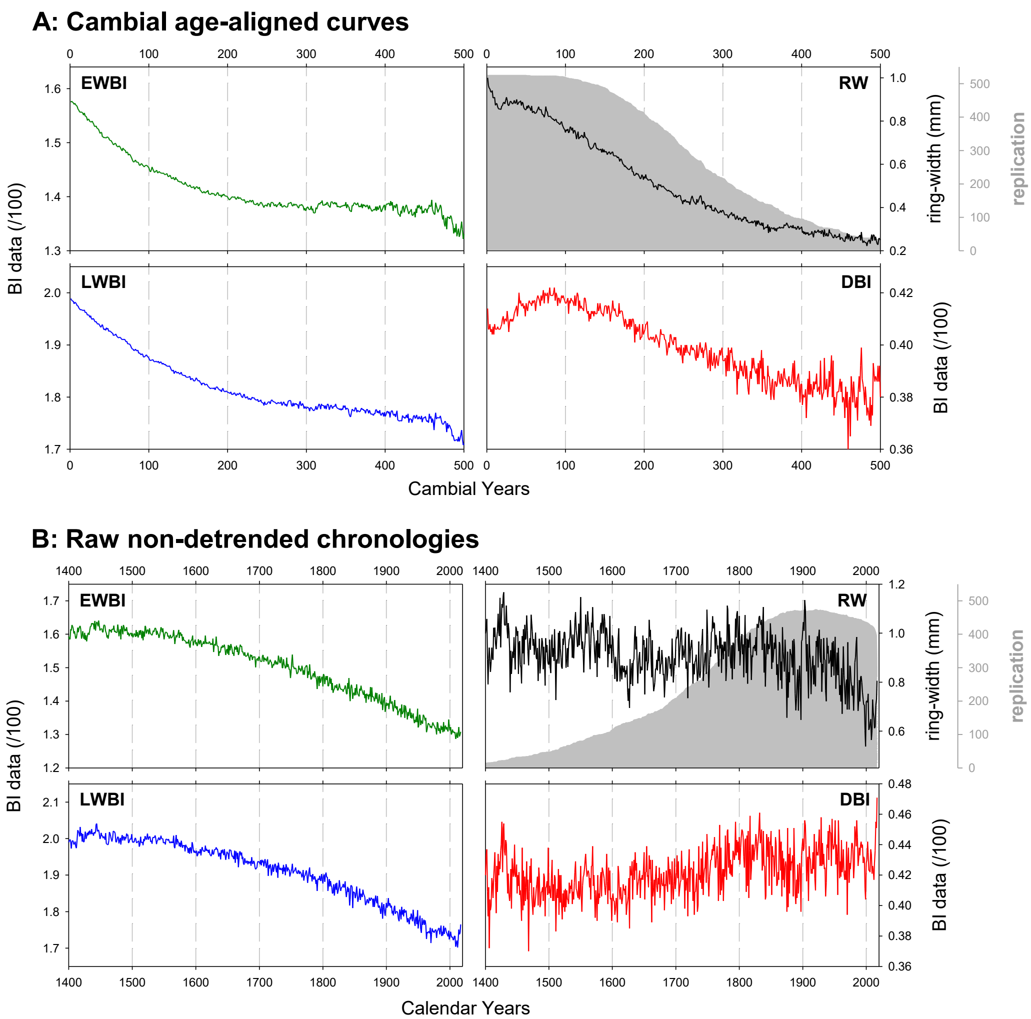

Figure A1: Different representations of the raw tree-ring parameter data; A: Cambial age aligned mean chronologies (pith offset information not used); B: raw non-detrended chronologies. Sample replication shown in the RW plots.

https://doi.org/10.5194/egusphere-2026-4785
Preprint. Discussion started: 28 August 2026

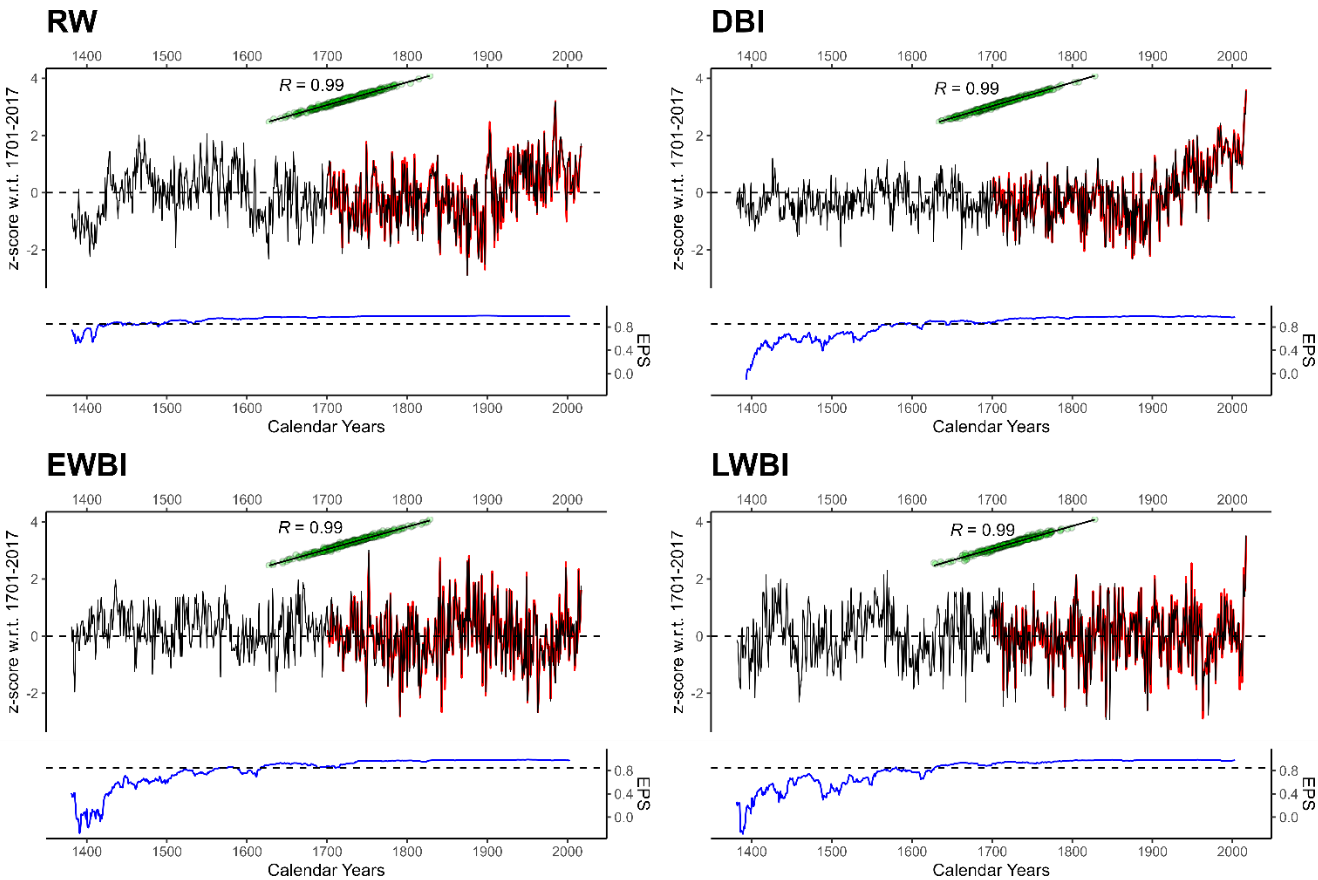

710 **Figure A2: Parameter specific PC1 scores (red) compared to regional parameter composite averages (black). The tree-ring data were detrended using an age-dependent spline (see methods). Scatter plot details the strong similarity of the two series justifying the use of the regional composite records. Lower plots (blue) denote running 30-year EPS values with 0.85 highlighted with a dashed line.**

https://doi.org/10.5194/egusphere-2026-4785
Preprint. Discussion started: 28 August 2026

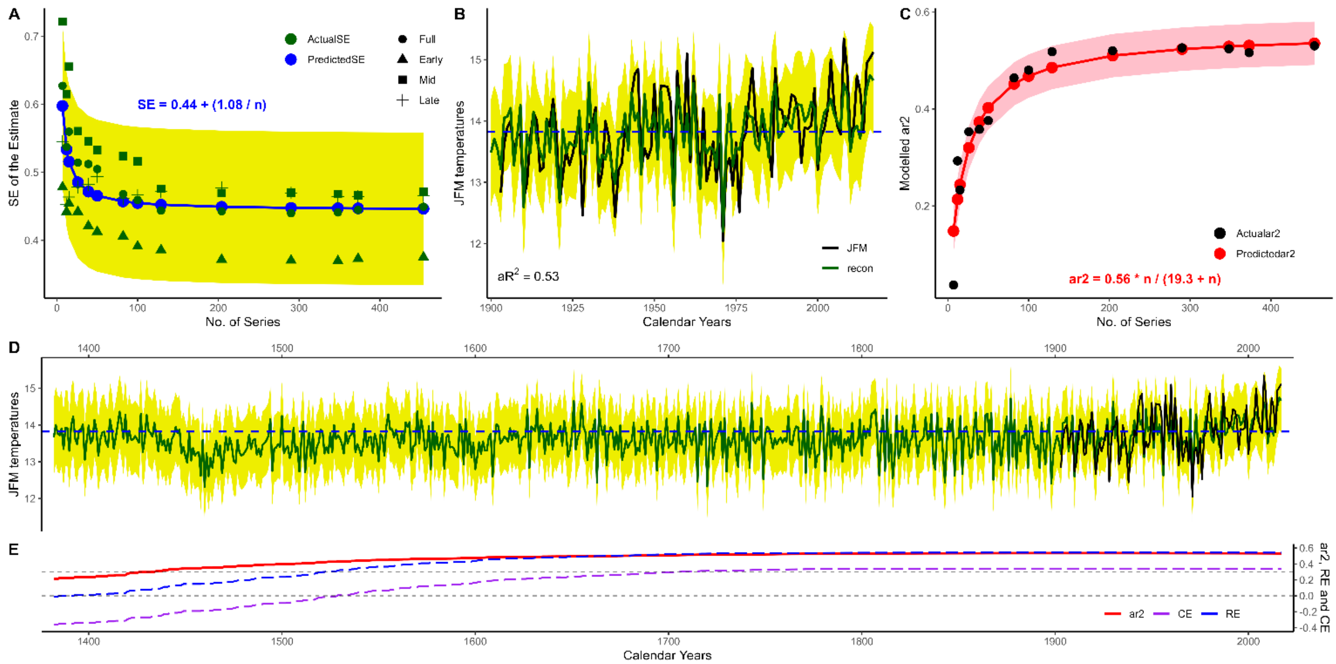

Figure A3: Pseudo-nested error modelling (Meko, 1997) for the NPAT reconstruction; A: Nested calibration modelling (1902-1931, 1932-1974, 1975-2017 and 1902-2017) of multiple nests from 1400, 1450, 1500, 1550, 1575, 1600, 1650, 1675, 1700, 1750, 1800, 1850, 1875 up to 2016 to model standard error (SE) of the regression estimate as a function of the changing number of input tree-ring series (Figure S1B); B: Full period regression calibration - actual and reconstructed values with 95% error envelope; C: as A, but non-linear modelling of the change in ar2 with varying replication (n); D: full NPAT reconstruction with 2-sigma error envelope; E: Modelled ar2 (based on 1902-2017 calibration) and RE / CE values (calculated on the 1902-1931 period based on 1932-2017 calibration) through time with 0 and 0.3 values highlighted with dashed line.

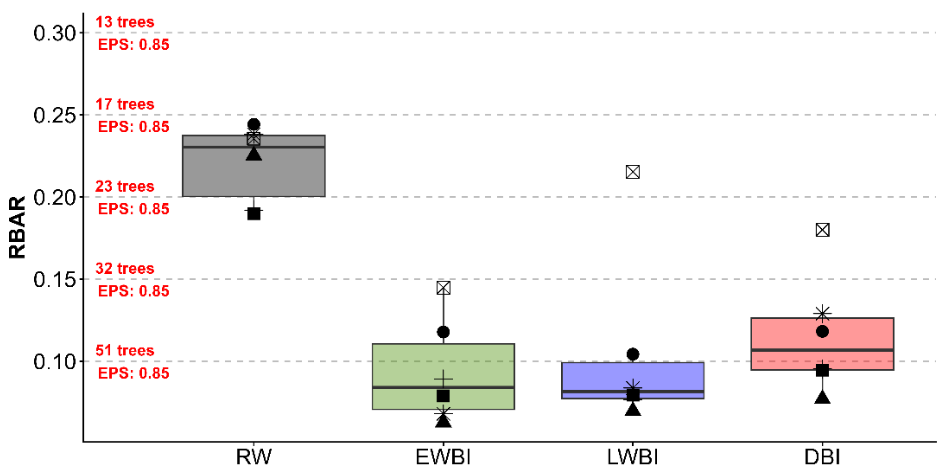

Figure A4: Chronology summary statistics for each site and variable using the age dependent spline (ADS) chronologies: A: Signal strength (mean inter-series correlation – RBAR). Horizontal dashed lines denote the number of trees needed to attain an Expressed Population Signal (EPS) greater than 0.85 for different RBAR levels.

https://doi.org/10.5194/egusphere-2026-4785
Preprint. Discussion started: 28 August 2026

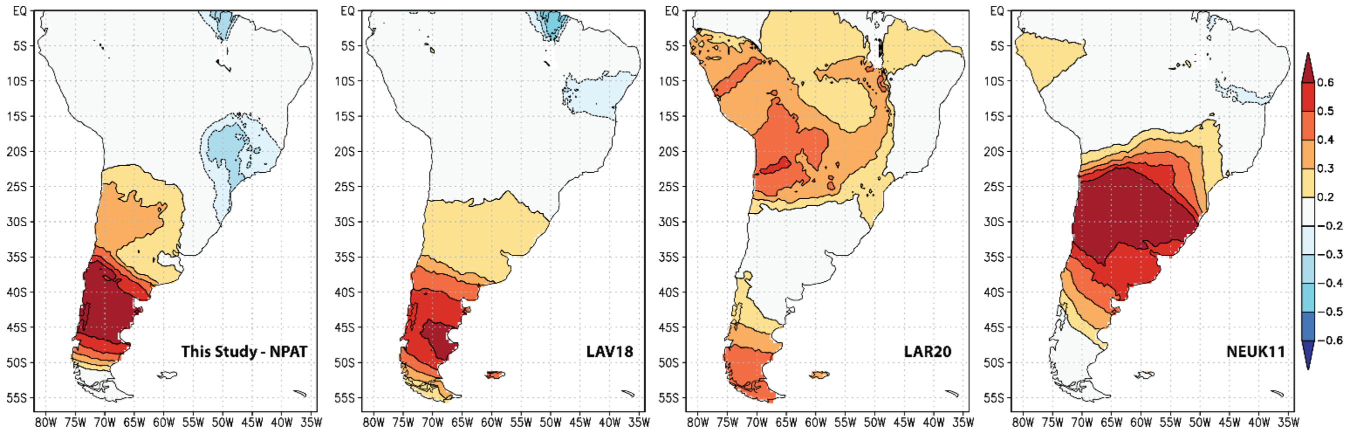

Figure A5: Spatial 1st differenced correlation plots (1902-1930) for each record utilising the original published calibration target summer season for each of the four-summer temperature reconstructions presented in Figure 7.

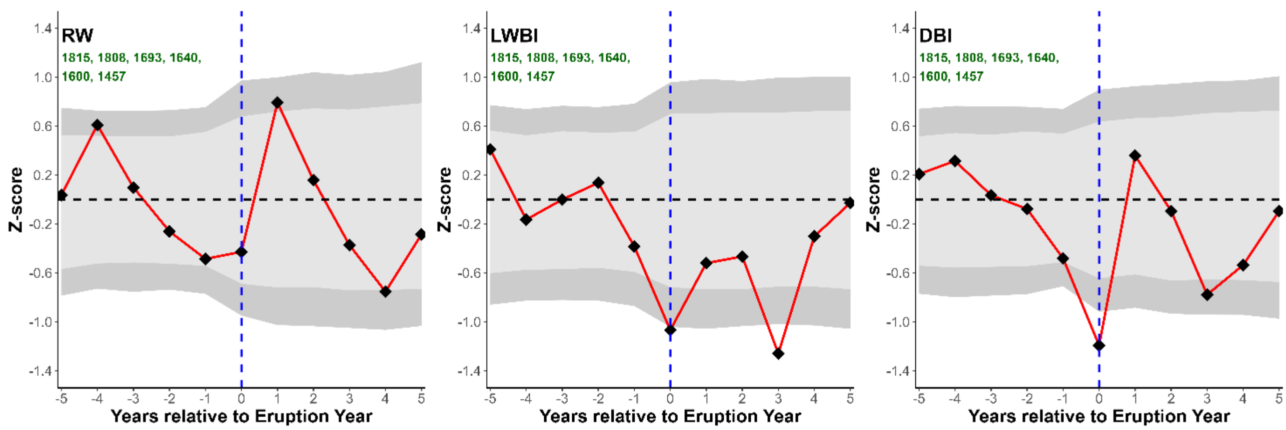

Figure A6: Superposed Epoch Analysis (Rao et al., 2019b) using the three regional composite tree-ring chronologies used to create the NPAT reconstruction. The dating of these TR records follows the Schulman shift convention (Schulman, 1956) – meaning, the low negative anomaly values appear 1 year earlier than the mean T+1 cooling response detailed in Figures 3 and 4. Note that the T+1 positive anomaly for RW is in line with its lagged previous year inverse response with summer temperatures (Mundo et al., 2024). This analysis focuses on tropical volcanic events with > 15 Tg S SSI (detailed in Table 2). All time-series were transformed to z-scores over the 1381-2016 common period before analysis.

https://doi.org/10.5194/egusphere-2026-4785
Preprint. Discussion started: 28 August 2026

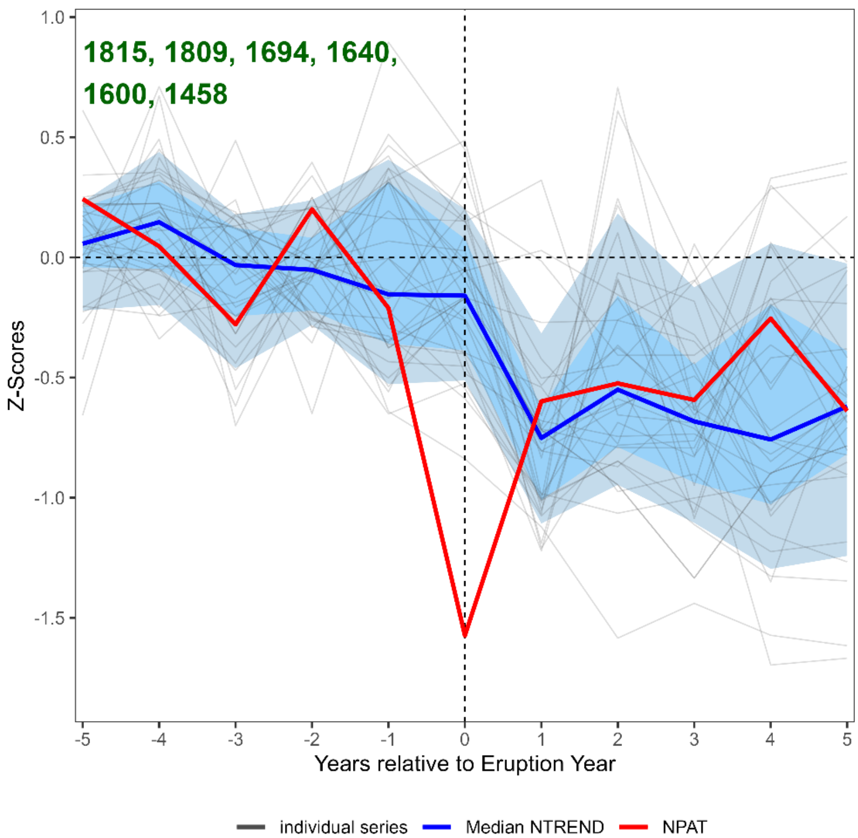

Figure A7: Comparison SEA analysis of NPAT with the individual N-TREND (Wilson et al., 2016) TR series as shown in Figure 10C, but the original "actual" eruption years for 1808, 1693 and 1457 have been shifted forward by 1 year portraying alternative dates of these eruptions within the uncertainties of the ice core records (see Appendix - Revised volcanic eruption dates for SEA). The blue line is the median of the individual N-TREND series SEA results while the inner and outer and light blue envelopes denote the 50% and 90% upper/lower percentiles of the N-TREND ensemble. The red line denoted the equivalent SEA results for the NPAT reconstruction.

Model + Reference	**Volcanic forcing**	**No. of simulations**
ACCESS-ESM1-5 (Ziehn et al., 2020)	Aerosol optical properties from eVolv2k	1
INM.INM-CM4-8 (Volodin et al., 2019)	Aerosol optical properties from eVolv2k	1
MRI-ESM2 (Yukimoto et al., 2019)	SO_2 injections from eVolv2k.	1
MIROC-ES2L (Ohgaito et al., 2021b)	Aerosol optical properties from evolv2k	1
MPI-ESM1-2-LR (van Dijk et al., 2024a; Mauritsen et al., 2019)	Aerosol optical properties from eVolv2k	2
UKESM1 (Marshall et al., 2024; Sellar et al., 2019)	SO_2 injections from eVolv2k plus temporal emissions for 1783 Laki	3

Table A1: Overview of PMIP4 past 1000-year model simulations using in the study

https://doi.org/10.5194/egusphere-2026-4785
Preprint. Discussion started: 28 August 2026

D4i	1884.4	1835.1	1815.8	1809.5	N/A	N/A	N/A	N/A	N/A
Summit_Composite	1884.0	1836.0	1816.0	1809.9	1694.2	1640.7	1600.9	1594.9	1459.0
NEEM-2011-S1	1883.6	1835.7	1815.6	1809.7	1695.0	1641.1	1601.1	1595.1	1459.1
Greenland	**1884.0**	**1835.6**	**1815.8**	**1809.7**	**1694.6**	**1640.9**	**1601.0**	**1595.0**	**1459.0**
WDC	1884.0	~~1834.7~~[a]	1815.4	1809.4	1694.6	1641.6	1600.4	1594.7	1458.4
LawDome	1884.5	1836.7	1815.8	1809.7	1695.3	1641.8	1600.7	1595.5	1458.5
DIV2010	1883.8	1835.7	1815.6	1809.5	N/A	N/A	N/A	N/A	N/A
Antarctica	**1884.1**	**1836.2**	**1815.6**	**1809.5**	**1695.0**	**1641.7**	**1600.6**	**1595.1**	**1458.5**
True eruption date (CE)	1883.63	1835.04	1815.29	N/A	N/A	1640.98	1600.13	N/A	N/A
Greenland mean time lag (yrs)	0.38	0.58	0.49	N/A	N/A	N/A[b]	0.86	N/A	N/A
Over all eruptions	**0.58 ± 0.20 (SD)**								
Antarctica mean time lag (yrs)	0.47	1.16	0.32	N/A	N/A	0.72	0.42	N/A	N/A
Over all eruptions	**0.52 ± 0.17 (SD)**								
Greenland projected mean eruption date (CE)	N/A	N/A	N/A	1809.1	1694.0	N/A	N/A	1594.4	1458.8
Antarctica projected mean eruption date (CE)	N/A	N/A	N/A	1809.0	1694.4	N/A	N/A	1594.6	1457.9
Recommended eruption age [estimated uncertainty]	**1883 [0]**	**1835 [0]**	**1815 [0]**	**1808 [+1]**	**1693 [+1]**	**1641 [0]**	**1600 [0]**	**1594 [±1]**	**1457 [+1]**

[a] excluded WDC value from the mean because the sulphur rise preceded the eruption date; [b] no time lag was calculated because the sulphate signal cannot confidently be attributed to Parker because of an additional major eruption in 1640 CE in Japan.

Table A2: Dating major volcanic eruptions in six polar high time-resolution ice-core records. Decimal year (CE) of volcanic sulphate deposition increase in sulphur and sulphate records from ice cores in Greenland (Fang et al., 2023; Keegan et al., 2014; Sigl et al., 2013; Stoffel et al., 2022) and Antarctica(Plummer et al., 2012; Sigl et al., 2013, 2014) following nine major eruptions. Mean time lag between volcanic sulphate deposition in Greenland and Antarctica, respectively, and the date of known eruption dates is calculated for each event; the mean time lag over all volcanic events for each ice-sheet is subtracted from the date of the volcanic sulphate increase from Greenland or Antarctica to derive projected mean dates for the unidentified major bipolar eruption signals; recommended ages are provided for the corresponding eruptions with their age uncertainties.

Code and data availability

Code availability: Although R scripts were used for analysis and visualisation, the methods employed were generally standard methods such as correlation, linear regression etc. The superposed epoch analysis code is published (Rao et al., 2019a). Specific code can however be provided on request to the corresponding author.

Data availability: in an Excel file we have provided the data for the NPAT reconstruction, the constituent regional parameter chronologies and model simulations used for the NPAT region, New Zealand and Tasmania. Note that the raw tree-ring data will be submitted and archived at the International Tree-Ring Data bank (https://www.ncei.noaa.gov/products/paleoclimatology/tree-ring)

Supplement link

The supplementary material is available online as separate file

Author Contribution

Rob Wilson: Project design – all aspects, paper writing and fieldwork
Ignacio Mundo: Project design – tree-ring data, paper writing and fieldwork
Lauren Marshall: Model data and paper writing
Emily Reid: Technician and paper editing
Michael Sigl: Project design – past eruption data and paper writing
Anja Schmidt: Model data and paper writing
Claudia Timmreck: Model data and paper writing
Shih-Wei Fang: Model data and paper writing
Rory Abernethy: Technician and paper editing
Valerie Daux Project design – tree-ring data, paper writing and fieldwork
Ricardo Villalba: Project design – tree-ring data, paper writing and fieldwork

Competing interests

The authors declare that they have no conflict of interest.

Disclaimer

"Copernicus Publications remains neutral with regard to jurisdictional claims made in the text, published maps, institutional affiliations, or any other geographical representation in this paper. While Copernicus Publications makes every effort to include appropriate place names, the final responsibility lies with the authors. Views expressed in the text are those of the authors and do not necessarily reflect the views of the publisher."

Financial support

RW, RV, IAM, VD: THEMES project funded by the BNP Paribas Foundation in the frame of its 'Climate Initiative' program."
RW, LM, AS: Natural Environment Research Council project Vol-Clim (NE/S000887/1)
RW: NSF-NERC (NE/W007223/1)
CT: Deutsche Forschungsgemeinschaft Research Unit VolImpact (FOR2820, Grant 398006378)
SWF: This work was supported by the Institute for Basic Science (IBS), Republic of Korea, under IBS-R028-D1.
IAM, RV: Mincyt, Argentina (Red Clima-Bosque contribution N° 8)
M.S. acknowledges the support of the ERC under the European Union’s Horizon 2020 research and innovation programme (grant agreement 820047).

References

Akaike, H.: A new look at the statistical model identification, IEEE Transactions on Automatic Control, 19, 716–723, https://doi.org/10.1109/TAC.1974.1100705, 1974.

Allen, K. J., Cook, E. R., Evans, R., Francey, R., Buckley, B. M., Palmer, J. G., Peterson, M. J., and Baker, P. J.: Lack of cool, not warm, extremes distinguishes late 20th Century climate in 979-year Tasmanian summer temperature reconstruction, Environ. Res. Lett., 13, 034041, https://doi.org/10.1088/1748-9326/aaafd7, 2018a.

Allen, K. J., Cook, E. R., Evans, R., Francey, R., Buckley, B. M., Palmer, J. G., Peterson, M. J., and Baker, P. J.: Lack of cool, not warm, extremes distinguishes late 20th Century climate in 979-year Tasmanian summer temperature reconstruction, Environ. Res. Lett., 13, 034041, https://doi.org/10.1088/1748-9326/aaafd7, 2018b.

Anchukaitis, K. J., Breitenmoser, P., Briffa, K. R., Buchwal, A., Büntgen, U., Cook, E. R., D’Arrigo, R. D., Esper, J., Evans, M. N., Frank, D., Grudd, H., Gunnarson, B. E., Hughes, M. K., Kirdyanov, A. V., Körner, C., Krusic, P. J., Luckman, B., Melvin, T. M., Salzer, M. W., Shashkin, A. V., Timmreck, C., Vaganov, E. A., and Wilson, R. J. S.: Tree rings and volcanic cooling, Nature Geosci, 5, 836–837, https://doi.org/10.1038/ngeo1645, 2012.

Anchukaitis, K. J., Wilson, R., Briffa, K. R., Büntgen, U., Cook, E. R., D’Arrigo, R., Davi, N., Esper, J., Frank, D., Gunnarson, B. E., Hegerl, G., Helama, S., Klesse, S., Krusic, P. J., Linderholm, H. W., Myglan, V., Osborn, T. J., Zhang, P., Rydval, M., Schneider, L., Schurer, A., Wiles, G., and Zorita, E.: Last millennium Northern Hemisphere summer temperatures from tree rings: Part II, spatially resolved reconstructions, Quaternary Science Reviews, 163, 1–22, https://doi.org/10.1016/j.quascirev.2017.02.020, 2017.

Archibald, A. T., O’Connor, F. M., Abraham, N. L., Archer-Nicholls, S., Chipperfield, M. P., Dalvi, M., Folberth, G. A., Dennison, F., Dhomse, S. S., Griffiths, P. T., Hardacre, C., Hewitt, A. J., Hill, R. S., Johnson, C. E., Keeble, J., Köhler, M. O., Morgenstern, O., Mulcahy, J. P., Ordóñez, C., Pope, R. J., Rumbold, S. T., Russo, M. R., Savage, N. H., Sellar, A., Stringer, M., Turnock, S. T., Wild, O., and Zeng, G.: Description and evaluation of the UKCA stratosphere–troposphere chemistry scheme (StratTrop vn 1.0) implemented in UKESM1, Geoscientific Model Development, 13, 1223–1266, https://doi.org/10.5194/gmd-13-1223-2020, 2020.

von Arx, G., Crivellaro, A., Prendin, A. L., Čufar, K., and Carrer, M.: Quantitative Wood Anatomy—Practical Guidelines, Front. Plant Sci., 7, https://doi.org/10.3389/fpls.2016.00781, 2016.

Björklund, J., von Arx, G., Nievergelt, D., Wilson, R., Van den Bulcke, J., Günther, B., Loader, N. J., Rydval, M., Fonti, P., Scharnweber, T., Andreu-Hayles, L., Büntgen, U., D'Arrigo, R., Davi, N., De Mil, T., Esper, J., Gärtner, H., Geary, J., Gunnarson, B. E., Hartl, C., Hevia, A., Song, H., Janecka, K., Kaczka, R. J., Kirdyanov, A. V., Kochbeck, M., Liu, Y., Meko, M., Mundo, I., Nicolussi, K., Oelkers, R., Pichler, T., Sánchez-Salguero, R., Schneider, L., Schweingruber, F., Timonen, M., Trouet, V., Van Acker, J., Verstege, A., Villalba, R., Wilmking, M., and Frank, D.: Scientific Merits and Analytical Challenges of Tree-Ring Densitometry, Reviews of Geophysics, 57, 1224–1264, https://doi.org/10.1029/2019RG000642, 2019.

Björklund, J., Seftigen, K., Fonti, P., Nievergelt, D., and von Arx, G.: Dendroclimatic potential of dendroanatomy in temperature-sensitive *Pinus sylvestris*, Dendrochronologia, 60, 125673, https://doi.org/10.1016/j.dendro.2020.125673, 2020.

Björklund, J., Seftigen, K., Stoffel, M., Fonti, M. V., Kottlow, S., Frank, D. C., Esper, J., Fonti, P., Goosse, H., Grudd, H., Gunnarson, B. E., Nievergelt, D., Pellizzari, E., Carrer, M., and von Arx, G.: Fennoscandian tree-ring anatomy shows a warmer modern than medieval climate, Nature, 620, 97–103, https://doi.org/10.1038/s41586-023-06176-4, 2023.

Björklund, J., Seftigen, K., Kaczka, R. J., Rydval, M., and Wilson, R.: A definition and standardised terminology for Blue Intensity from Conifers, Dendrochronologia, 85, 126200, https://doi.org/10.1016/j.dendro.2024.126200, 2024.

Björklund, J. A., Gunnarson, B. E., Seftigen, K., Esper, J., and Linderholm, H. W.: Blue intensity and density from northern Fennoscandian tree rings, exploring the potential to improve summer temperature reconstructions with earlywood information, Climate of the Past, 10, 877–885, https://doi.org/10.5194/cp-10-877-2014, 2014.

Blake, S. A. P., Palmer, J. G., Björklund, J., Harper, J. B., and Turney, C. S. M.: Palaeoclimate potential of New Zealand *Manoao colensoi* (silver pine) tree rings using Blue-Intensity (BI), Dendrochronologia, 60, 125664, https://doi.org/10.1016/j.dendro.2020.125664, 2020.

Boninsegna, J. and Hughes, M.: Volcanic Signals in Temperature Reconstructions Based on Tree-Ring Records for North and South America, in: Interhemispheric Climate Linkages, 141–154, https://doi.org/10.1016/B978-012472670-3/50012-4, 2001.

Boninsegna, J. A., Argollo, J., Aravena, J. C., Barichivich, J., Christie, D., Ferrero, M. E., Lara, A., Le Quesne, C., Luckman, B. H., Masiokas, M., Morales, M., Oliveira, J. M., Roig, F., Srur, A., and Villalba, R.: Dendroclimatological reconstructions in South America: A review, Palaeogeography, Palaeoclimatology, Palaeoecology, 281, 210–228, https://doi.org/10.1016/j.palaeo.2009.07.020, 2009.

Briffa, K. R., Jones, P. D., Schweingruber, F. H., and Osborn, T. J.: Influence of volcanic eruptions on Northern Hemisphere summer temperature over the past 600 years, Nature, 393, 450–455, https://doi.org/10.1038/30943, 1998.

Brookhouse, M. and Graham, R.: Application of the Minimum Blue-Intensity Technique To A Southern-Hemisphere Conifer, Tree-Ring Research, 72, 103–107, https://doi.org/10.3959/1536-1098-72.02.103, 2016.

Buckley, B. M., Hansen, K. G., Griffin, K. L., Schmiege, S., Oelkers, R., D'Arrigo, R. D., Stahle, D. K., Davi, N., Nguyen, T. Q. T., Le, C. N., and Wilson, R. J. S.: Blue intensity from a tropical conifer's annual rings for climate reconstruction: An ecophysiological perspective, Dendrochronologia, 50, 10–22, https://doi.org/10.1016/j.dendro.2018.04.003, 2018.

Burke, A., Innes, H. M., Crick, L., Anchukaitis, K. J., Byrne, M. P., Hutchison, W., McConnell, J. R., Moore, K. A., Rae, J. W. B., Sigl, M., and Wilson, R.: High sensitivity of summer temperatures to stratospheric sulfur loading from volcanoes in the Northern Hemisphere, Proceedings of the National Academy of Sciences, 120, e2221810120, https://doi.org/10.1073/pnas.2221810120, 2023.

https://doi.org/10.5194/egusphere-2026-4785
Preprint. Discussion started: 28 August 2026

Campbell, R., McCarroll, D., Loader, N. J., Grudd, H., Robertson, I., and Jalkanen, R.: Blue intensity in Pinus sylvestris tree-rings: developing a new palaeoclimate proxy, The Holocene, 17, 821–828, https://doi.org/10.1177/0959683607080523, 2007.

Cook, E., Bird, T., Peterson, M., Barbetti, M., Buckley, B., D'Arrigo, R., and Francey, R.: Climatic change over the last millennium in Tasmania reconstructed from tree-rings, The Holocene, 2, 205–217, https://doi.org/10.1177/095968369200200302, 1992.

Cook, E. R., Briffa, K. R., Шиятов, С. Г., and Мазепа, В. С.: Tree-ring standardization and growth-trend estimation, 104–123, 1990.

Cook, E. R., Briffa, K. R., Meko, D. M., Graybill, D. A., and Funkhouser, G.: The "segment length curse" in long tree-ring chronology development for palaeoclimatic studies, The Holocene, 5, 229–237, https://doi.org/10.1177/095968369500500211, 1995.

Cook, E. R., Meko, D. M., Stahle, D. W., and Cleaveland, M. K.: Drought Reconstructions for the Continental United States, 1999.

Cook, E. R., Buckley, B. M., D'Arrigo, R. D., and Peterson, M. J.: Warm-season temperatures since 1600 BC reconstructed from Tasmanian tree rings and their relationship to large-scale sea surface temperature anomalies, Climate Dynamics, 16, 79–91, https://doi.org/10.1007/s003820050006, 2000.

Cook, E. R., Palmer, J. G., and D'Arrigo, R. D.: Evidence for a 'Medieval Warm Period' in a 1,100 year tree-ring reconstruction of past austral summer temperatures in New Zealand, Geophysical Research Letters, 29, 12-1-12–4, https://doi.org/10.1029/2001GL014580, 2002.

Crowley, T. J. and Unterman, M. B.: Technical details concerning development of a 1200 yr proxy index for global volcanism, Earth System Science Data, 5, 187–197, https://doi.org/10.5194/essd-5-187-2013, 2013.

D'Arrigo, R., Wilson, R., and Anchukaitis, K. J.: Volcanic cooling signal in tree ring temperature records for the past millennium, Journal of Geophysical Research: Atmospheres, 118, 9000–9010, https://doi.org/10.1002/jgrd.50692, 2013.

van Dijk, E. J. C., Jungclaus, J., Sigl, M., Timmreck, C., and Krüger, K.: High-frequency climate forcing causes prolonged cold periods in the Holocene, Commun Earth Environ, 5, 1–9, https://doi.org/10.1038/s43247-024-01380-0, 2024a.

van Dijk, E. J. C., Jungclaus, J., Sigl, M., Timmreck, C., and Krüger, K.: High-frequency climate forcing causes prolonged cold periods in the Holocene, Commun Earth Environ, 5, 1–9, https://doi.org/10.1038/s43247-024-01380-0, 2024b.

Esper, J., Frank, D. C., Wilson, R. J. S., and Briffa, K. R.: Effect of scaling and regression on reconstructed temperature amplitude for the past millennium, Geophysical Research Letters, 32, https://doi.org/10.1029/2004GL021236, 2005.

Esper, J., Düthorn, E., Krusic, P. J., Timonen, M., and Büntgen, U.: Northern European summer temperature variations over the Common Era from integrated tree-ring density records, Journal of Quaternary Science, 29, 487–494, https://doi.org/10.1002/jqs.2726, 2014.

Esper, J., Schneider, L., Smerdon, J. E., Schöne, B. R., and Büntgen, U.: Signals and memory in tree-ring width and density data, Dendrochronologia, 35, 62–70, https://doi.org/10.1016/j.dendro.2015.07.001, 2015.

https://doi.org/10.5194/egusphere-2026-4785
Preprint. Discussion started: 28 August 2026

Falvey, M. and Garreaud, R. D.: Regional cooling in a warming world: Recent temperature trends in the southeast Pacific and along the west coast of subtropical South America (1979–2006), Journal of Geophysical Research: Atmospheres, 114, https://doi.org/10.1029/2008JD010519, 2009.

Fang, S.-W., Timmreck, C., Jungclaus, J., Krüger, K., and Schmidt, H.: On the additivity of climate responses to the volcanic and solar forcing in the early 19th century, Earth System Dynamics, 13, 1535–1555, https://doi.org/10.5194/esd-13-1535-2022, 2022.

Fang, S.-W., Sigl, M., Toohey, M., Jungclaus, J., Zanchettin, D., and Timmreck, C.: The Role of Small to Moderate Volcanic Eruptions in the Early 19th Century Climate, Geophysical Research Letters, 50, e2023GL105307, https://doi.org/10.1029/2023GL105307, 2023.

Fogt, R. L. and Marshall, G. J.: The Southern Annular Mode: Variability, trends, and climate impacts across the Southern Hemisphere, WIREs Climate Change, 11, e652, https://doi.org/10.1002/wcc.652, 2020.

Fox, J.: Applied regression analysis, linear models, and related methods, Sage Publications, Inc, Thousand Oaks, CA, US, xxi, 597 pp., 1997.

Franke, J., Valler, V., Brönnimann, S., Neukom, R., and Jaume-Santero, F.: The importance of input data quality and quantity in climate field reconstructions – results from the assimilation of various tree-ring collections, Climate of the Past, 16, 1061–1074, https://doi.org/10.5194/cp-16-1061-2020, 2020.

Fuentes, M., Salo, R., Björklund, J., Seftigen, K., Zhang, P., Gunnarson, B., Aravena, J.-C., and Linderholm, H. W.: A 970-year-long summer temperature reconstruction from Rogen, west-central Sweden, based on blue intensity from tree rings, The Holocene, 28, 254–266, https://doi.org/10.1177/0959683617721322, 2018.

Gao, C., Robock, A., and Ammann, C.: Volcanic forcing of climate over the past 1500 years: An improved ice core-based index for climate models, Journal of Geophysical Research: Atmospheres, 113, https://doi.org/10.1029/2008JD010239, 2008.

Guevara-Murua, A., Williams, C. A., Hendy, E. J., Rust, A. C., and Cashman, K. V.: Observations of a stratospheric aerosol *veil* from a tropical volcanic eruption in December 1808: is this the *Unknown* ∼1809 eruption?, Climate of the Past, 10, 1707–1722, https://doi.org/10.5194/cp-10-1707-2014, 2014.

Guillet, S., Corona, C., Stoffel, M., Khodri, M., Lavigne, F., Ortega, P., Eckert, N., Sielenou, P. D., Daux, V., Churakova (Sidorova), O. V., Davi, N., Edouard, J.-L., Zhang, Y., Luckman, B. H., Myglan, V. S., Guiot, J., Beniston, M., Masson-Delmotte, V., and Oppenheimer, C.: Climate response to the Samalas volcanic eruption in 1257 revealed by proxy records, Nature Geosci, 10, 123–128, https://doi.org/10.1038/ngeo2875, 2017.

Harris, I., Osborn, T. J., Jones, P., and Lister, D.: Version 4 of the CRU TS monthly high-resolution gridded multivariate climate dataset, Sci Data, 7, 109, https://doi.org/10.1038/s41597-020-0453-3, 2020.

Harvey, P. J. and Grab, S. W.: Southern Hemisphere continental temperature responses to major volcanic eruptions since 1883 in CMIP5 models, Theor Appl Climatol, 147, 143–157, https://doi.org/10.1007/s00704-021-03810-x, 2022.

Harvey, P. J., Grab, S. W., and Malherbe, J.: Major Volcanic Eruptions and Their Impacts on Southern Hemisphere Temperatures During the Late 19th and 20th Centuries, as Simulated by CMIP5 Models, Geophysical Research Letters, 47, e2020GL087792, https://doi.org/10.1029/2020GL087792, 2020.

Heeter, K. J., King, D. J., Harley, G. L., and Kaczka, R. J.: Video tutorial: Measuring blue intensity with the CooRecorder software application, Dendrochronologia, 76, 125999, https://doi.org/10.1016/j.dendro.2022.125999, 2022.

Heeter, K. J., Harley, G. L., Abatzoglou, J. T., Anchukaitis, K. J., Cook, E. R., Coulthard, B. L., Dye, L. A., and Homfeld, I. K.: Unprecedented 21st century heat across the Pacific Northwest of North America, npj Clim Atmos Sci, 6, 1–9, https://doi.org/10.1038/s41612-023-00340-3, 2023.

Hegerl, G. and Zwiers, F.: Use of models in detection and attribution of climate change, WIREs Climate Change, 2, 570–591, https://doi.org/10.1002/wcc.121, 2011.

Higgins, P. A., Palmer, J. G., Turney, C. S. M., Andersen, M. S., and Johnson, F.: Do Southern Hemisphere tree rings record past volcanic events? A case study from New Zealand, Climate of the Past, 18, 1169–1188, https://doi.org/10.5194/cp-18-1169-2022, 2022.

Holmes, R.: Computer-Assisted Quality Control in Tree-Ring Dating and Measurement, Tree-Ring Bulletin, 43, 51–57, 1983.

Jungclaus, J. H., Bard, E., Baroni, M., Braconnot, P., Cao, J., Chini, L. P., Egorova, T., Evans, M., González-Rouco, J. F., Goosse, H., Hurtt, G. C., Joos, F., Kaplan, J. O., Khodri, M., Klein Goldewijk, K., Krivova, N., LeGrande, A. N., Lorenz, S. J., Luterbacher, J., Man, W., Maycock, A. C., Meinshausen, M., Moberg, A., Muscheler, R., Nehrbass-Ahles, C., Otto-Bliesner, B. I., Phipps, S. J., Pongratz, J., Rozanov, E., Schmidt, G. A., Schmidt, H., Schmutz, W., Schurer, A., Shapiro, A. I., Sigl, M., Smerdon, J. E., Solanki, S. K., Timmreck, C., Toohey, M., Usoskin, I. G., Wagner, S., Wu, C.-J., Yeo, K. L., Zanchettin, D., Zhang, Q., and Zorita, E.: The PMIP4 contribution to CMIP6 – Part 3: The last millennium, scientific objective, and experimental design for the PMIP4 *past1000* simulations, Geoscientific Model Development, 10, 4005–4033, https://doi.org/10.5194/gmd-10-4005-2017, 2017.

Keegan, K. M., Albert, M. R., McConnell, J. R., and Baker, I.: Climate change and forest fires synergistically drive widespread melt events of the Greenland Ice Sheet, Proceedings of the National Academy of Sciences, 111, 7964–7967, https://doi.org/10.1073/pnas.1405397111, 2014.

King, J. M., Anchukaitis, K. J., Tierney, J. E., Hakim, G. J., Emile-Geay, J., Zhu, F., and Wilson, R.: A Data Assimilation Approach to Last Millennium Temperature Field Reconstruction Using a Limited High-Sensitivity Proxy Network, https://doi.org/10.1175/JCLI-D-20-0661.1, 2021.

Lara, A. and Villalba, R.: A 3620-Year Temperature Record from Fitzroya cupressoides Tree Rings in Southern South America, Science, 260, 1104–1106, https://doi.org/10.1126/science.260.5111.1104, 1993.

Lara, A., Villalba, R., Urrutia-Jalabert, R., González-Reyes, A., Aravena, J. C., Luckman, B. H., Cuq, E., Rodríguez, C., and Wolodarsky-Franke, A.: +A 5680-year tree-ring temperature record for southern South America, Quaternary Science Reviews, 228, 106087, https://doi.org/10.1016/j.quascirev.2019.106087, 2020.

Lavergne, A., Daux, V., Pierre, M., Stievenard, M., Srur, A. M., and Villalba, R.: Past Summer Temperatures Inferred From Dendrochronological Records of on the Eastern Slope of the Northern Patagonian Andes, Journal of Geophysical Research: Biogeosciences, 123, 32–45, https://doi.org/10.1002/2017JG003989, 2018.

Lücke, L. J., Hegerl, G. C., Schurer, A. P., and Wilson, R.: Effects of Memory Biases on Variability of Temperature Reconstructions, https://doi.org/10.1175/JCLI-D-19-0184.1, 2019.

https://doi.org/10.5194/egusphere-2026-4785
Preprint. Discussion started: 28 August 2026

Lücke, L. J., Schurer, A. P., Toohey, M., Marshall, L. R., and Hegerl, G. C.: The effect of uncertainties in natural forcing records on simulated temperature during the last millennium, Climate of the Past, 19, 959–978, https://doi.org/10.5194/cp-19-959-2023, 2023.

Luterbacher, J. and Pfister, C.: The year without a summer, Nature Geosci, 8, 246–248, https://doi.org/10.1038/ngeo2404, 2015.

Mann, G. W., Carslaw, K. S., Spracklen, D. V., Ridley, D. A., Manktelow, P. T., Chipperfield, M. P., Pickering, S. J., and Johnson, C. E.: Description and evaluation of GLOMAP-mode: a modal global aerosol microphysics model for the UKCA composition-climate model, Geoscientific Model Development, 3, 519–551, https://doi.org/10.5194/gmd-3-519-2010, 2010.

Mann, M. E., Fuentes, J. D., and Rutherford, S.: Underestimation of volcanic cooling in tree-ring-based reconstructions of hemispheric temperatures, Nature Geosci, 5, 202–205, https://doi.org/10.1038/ngeo1394, 2012.

Marshall, L., Schmidt, A., Toohey, M., Carslaw, K. S., Mann, G. W., Sigl, M., Khodri, M., Timmreck, C., Zanchettin, D., Ball, W. T., Bekki, S., Brooke, J. S. A., Dhomse, S., Johnson, C., Lamarque, J.-F., LeGrande, A. N., Mills, M. J., Niemeier, U., Pope, J. O., Poulain, V., Robock, A., Rozanov, E., Stenke, A., Sukhodolov, T., Tilmes, S., Tsigaridis, K., and Tummon, F.: Multi-model comparison of the volcanic sulfate deposition from the 1815 eruption of Mt. Tambora, Atmospheric Chemistry and Physics, 18, 2307–2328, https://doi.org/10.5194/acp-18-2307-2018, 2018.

Marshall, L. R., Schmidt, A., Johnson, J. S., Mann, G. W., Lee, L. A., Rigby, R., and Carslaw, K. S.: Unknown Eruption Source Parameters Cause Large Uncertainty in Historical Volcanic Radiative Forcing Reconstructions, Journal of Geophysical Research: Atmospheres, 126, e2020JD033578, https://doi.org/10.1029/2020JD033578, 2021.

Marshall, L. R., Schmidt, A., Schurer, A. P., Abraham, N. L., Lücke, L. J., Wilson, R., Anchukaitis, K., Hegerl, G., Johnson, B., Otto-Bliesner, B. L., Brady, E. C., Khodri, M., and Yoshida, K.: Last Millennium Volcanic Forcing and Climate Response using SO_2 Emissions, EGUsphere, 1–39, https://doi.org/10.5194/egusphere-2024-1322, 2024.

Marshall, L. R., Schmidt, A., Schurer, A. P., Abraham, N. L., Lücke, L. J., Wilson, R., Anchukaitis, K. J., Hegerl, G. C., Johnson, B., Otto-Bliesner, B. L., Brady, E. C., Khodri, M., and Yoshida, K.: Last-millennium volcanic forcing and climate response using SO_2 emissions, Climate of the Past, 21, 161–184, https://doi.org/10.5194/cp-21-161-2025, 2025.

Matskovsky, V. V. and Helama, S.: Testing long-term summer temperature reconstruction based on maximum density chronologies obtained by reanalysis of tree-ring data sets from northernmost Sweden and Finland, Climate of the Past, 10, 1473–1487, https://doi.org/10.5194/cp-10-1473-2014, 2014.

Mauritsen, T., Bader, J., Becker, T., Behrens, J., Bittner, M., Brokopf, R., Brovkin, V., Claussen, M., Crueger, T., Esch, M., Fast, I., Fiedler, S., Fläschner, D., Gayler, V., Giorgetta, M., Goll, D. S., Haak, H., Hagemann, S., Hedemann, C., Hohenegger, C., Ilyina, T., Jahns, T., Jimenéz-de-la-Cuesta, D., Jungclaus, J., Kleinen, T., Kloster, S., Kracher, D., Kinne, S., Kleberg, D., Lasslop, G., Kornblueh, L., Marotzke, J., Matei, D., Meraner, K., Mikolajewicz, U., Modali, K., Möbis, B., Müller, W. A., Nabel, J. E. M. S., Nam, C. C. W., Notz, D., Nyawira, S.-S., Paulsen, H., Peters, K., Pincus, R., Pohlmann, H., Pongratz, J., Popp, M., Raddatz, T. J., Rast, S., Redler, R., Reick, C. H., Rohrschneider, T., Schemann, V., Schmidt, H., Schnur, R., Schulzweida, U., Six, K. D., Stein, L., Stemmler, I., Stevens, B., von Storch, J.-S., Tian, F., Voigt, A., Vrese, P., Wieners, K.-H., Wilkenskjeld, S., Winkler, A., and Roeckner, E.: Developments in the MPI-M Earth System Model version 1.2 (MPI-ESM1.2) and Its Response to Increasing CO2, Journal of Advances in Modeling Earth Systems, 11, 998–1038, https://doi.org/10.1029/2018MS001400, 2019.

Maxwell, R. S. and Larsson, L.-A.: Measuring tree-ring widths using the CooRecorder software application, Dendrochronologia, 67, 125841, https://doi.org/10.1016/j.dendro.2021.125841, 2021.

https://doi.org/10.5194/egusphere-2026-4785
Preprint. Discussion started: 28 August 2026

Meier, W. J.-H., Aravena, J.-C., Jaña, R., Braun, M. H., Hochreuther, P., Soto-Rogel, P., and Grießinger, J.: A tree-ring δ18O series from southernmost Fuego-Patagonia is recording flavors of the Antarctic Oscillation, Global and Planetary Change, 195, 103302, https://doi.org/10.1016/j.gloplacha.2020.103302, 2020.

Meko, D.: Dendroclimatic Reconstruction with Time Varying Predictor Subsets of Tree Indices, 1997.

Melvin, T. M. and Briffa, K. R.: A "signal-free" approach to dendroclimatic standardisation, Dendrochronologia, 26, 71–86, https://doi.org/10.1016/j.dendro.2007.12.001, 2008.

Melvin, T. M., Briffa, K. R., Nicolussi, K., and Grabner, M.: Time-varying-response smoothing, Dendrochronologia, 25, 65–69, https://doi.org/10.1016/j.dendro.2007.01.004, 2007.

Mulcahy, J. P., Jones, C. G., Rumbold, S. T., Kuhlbrodt, T., Dittus, A. J., Blockley, E. W., Yool, A., Walton, J., Hardacre, C., Andrews, T., Bodas-Salcedo, A., Stringer, M., de Mora, L., Harris, P., Hill, R., Kelley, D., Robertson, E., and Tang, Y.: UKESM1.1: development and evaluation of an updated configuration of the UK Earth System Model, Geoscientific Model Development, 16, 1569–1600, https://doi.org/10.5194/gmd-16-1569-2023, 2023.

Mundo, I. A., Roig Juñent, F. A., Villalba, R., Kitzberger, T., and Barrera, M. D.: Araucaria araucana tree-ring chronologies in Argentina: spatial growth variations and climate influences, Trees, 26, 443–458, https://doi.org/10.1007/s00468-011-0605-3, 2012.

Mundo, I. A., Villalba, R., Velez, S., and Wilson, R.: Blue intensity measurements in a South American conifer: evaluation of different methodological approaches for *Araucaria araucana*, Dendrochronologia, 84, 126177, https://doi.org/10.1016/j.dendro.2024.126177, 2024.

Neukom, R., Luterbacher, J., Villalba, R., Küttel, M., Frank, D., Jones, P. D., Grosjean, M., Wanner, H., Aravena, J.-C., Black, D. E., Christie, D. A., D'Arrigo, R., Lara, A., Morales, M., Soliz-Gamboa, C., Srur, A., Urrutia, R., and von Gunten, L.: Multiproxy summer and winter surface air temperature field reconstructions for southern South America covering the past centuries, Clim Dyn, 37, 35–51, https://doi.org/10.1007/s00382-010-0793-3, 2011.

Neukom, R., Gergis, J., Karoly, D. J., Wanner, H., Curran, M., Elbert, J., González-Rouco, F., Linsley, B. K., Moy, A. D., Mundo, I., Raible, C. C., Steig, E. J., van Ommen, T., Vance, T., Villalba, R., Zinke, J., and Frank, D.: Inter-hemispheric temperature variability over the past millennium, Nature Clim Change, 4, 362–367, https://doi.org/10.1038/nclimate2174, 2014.

O'Connor, J. A., Henley, B. J., Brookhouse, M. T., and Allen, K. J.: Ring-width and blue-light chronologies of *Podocarpus lawrencei* from southeastern mainland Australia reveal a regional climate signal, Climate of the Past, 18, 2567–2581, https://doi.org/10.5194/cp-18-2567-2022, 2022.

Ohgaito, R., Yamamoto, A., Hajima, T., O'ishi, R., Abe, M., Tatebe, H., Abe-Ouchi, A., and Kawamiya, M.: PMIP4 experiments using MIROC-ES2L Earth system model, Geoscientific Model Development, 14, 1195–1217, https://doi.org/10.5194/gmd-14-1195-2021, 2021a.

Ohgaito, R., Yamamoto, A., Hajima, T., O'ishi, R., Abe, M., Tatebe, H., Abe-Ouchi, A., and Kawamiya, M.: PMIP4 experiments using MIROC-ES2L Earth system model, Geoscientific Model Development, 14, 1195–1217, https://doi.org/10.5194/gmd-14-1195-2021, 2021b.

Oppenheimer, C.: Climatic, environmental and human consequences of the largest known historic eruption: Tambora volcano (Indonesia) 1815, Progress in Physical Geography: Earth and Environment, 27, 230–259, https://doi.org/10.1191/0309133303pp379ra, 2003.

Penchenat, T., Daux, V., Mundo, I., Pierre, M., Stievenard, M., Srur, A., Andreu-Hayles, L., and Villalba, R.: Tree-ring isotopes from *Araucaria araucana* as useful proxies for climate reconstructions, Dendrochronologia, 74, 125979, https://doi.org/10.1016/j.dendro.2022.125979, 2022.

Plummer, C. T., Curran, M. a. J., van Ommen, T. D., Rasmussen, S. O., Moy, A. D., Vance, T. R., Clausen, H. B., Vinther, B. M., and Mayewski, P. A.: An independently dated 2000-yr volcanic record from Law Dome, East Antarctica, including a new perspective on the dating of the 1450s CE eruption of Kuwae, Vanuatu, Climate of the Past, 8, 1929–1940, https://doi.org/10.5194/cp-8-1929-2012, 2012.

Rao, M. P., Cook, E. R., Cook, B. I., Anchukaitis, K. J., D'Arrigo, R. D., Krusic, P. J., and LeGrande, A. N.: A double bootstrap approach to Superposed Epoch Analysis to evaluate response uncertainty, Dendrochronologia, 55, 119–124, https://doi.org/10.1016/j.dendro.2019.05.001, 2019a.

Rao, M. P., Cook, E. R., Cook, B. I., Anchukaitis, K. J., D'Arrigo, R. D., Krusic, P. J., and LeGrande, A. N.: A double bootstrap approach to Superposed Epoch Analysis to evaluate response uncertainty, Dendrochronologia, 55, 119–124, https://doi.org/10.1016/j.dendro.2019.05.001, 2019b.

Reid, E. and Wilson, R.: Delta blue intensity vs. maximum density: A case study using *Pinus uncinata* in the Pyrenees, Dendrochronologia, 61, 125706, https://doi.org/10.1016/j.dendro.2020.125706, 2020.

Ro, S., Hur, S. D., Ekaykin, A., Han, Y., Ro, C.-U., Hong, S.-B., Lee, M. J., Chang, C., Lee, S., Moon, J., Jung, H., Veres, A., Lee, A., and Hong, S.: Origin of the 1458/59 CE volcanic eruption revealed through analysis of glass shards in the firn core from Antarctic Vostok station, Commun Earth Environ, 6, 828, https://doi.org/10.1038/s43247-025-02797-x, 2025.

Robock, A. and Mao, J.: The Volcanic Signal in Surface Temperature Observations, Journal of Climate, 8, 1086–1103, https://doi.org/10.1175/1520-0442(1995)008%3C1086:TVSIST%3E2.0.CO;2, 1995.

Rydval, M., Larsson, L.-Å., McGlynn, L., Gunnarson, B. E., Loader, N. J., Young, G. H. F., and Wilson, R.: Blue intensity for dendroclimatology: Should we have the blues? Experiments from Scotland, Dendrochronologia, 32, 191–204, https://doi.org/10.1016/j.dendro.2014.04.003, 2014.

Rydval, M., Loader, N. J., Gunnarson, B. E., Druckenbrod, D. L., Linderholm, H. W., Moreton, S. G., Wood, C. V., and Wilson, R.: Reconstructing 800 years of summer temperatures in Scotland from tree rings, Clim Dyn, 49, 2951–2974, https://doi.org/10.1007/s00382-016-3478-8, 2017.

Rydval, M., Björklund, J., von Arx, G., Begović, K., Lexa, M., Nogueira, J., Schurman, J. S., and Jiang, Y.: Ultra-high-resolution reflected-light imaging for dendrochronology, Dendrochronologia, 83, 126160, https://doi.org/10.1016/j.dendro.2023.126160, 2024.

Schneider, L., Smerdon, J. E., Büntgen, U., Wilson, R. J. S., Myglan, V. S., Kirdyanov, A. V., and Esper, J.: Revising midlatitude summer temperatures back to A.D. 600 based on a wood density network, Geophysical Research Letters, 42, 4556–4562, https://doi.org/10.1002/2015GL063956, 2015.

Schulman, E.: Dendroclimatic Changes in Semiarid America, Univ. of Arizona Press, Tucson, 142 pp., 1956.

Schurer, A. P., Tett, S. F. B., and Hegerl, G. C.: Small influence of solar variability on climate over the past millennium, Nature Geosci, 7, 104–108, https://doi.org/10.1038/ngeo2040, 2014.

Sellar, A. A., Jones, C. G., Mulcahy, J. P., Tang, Y., Yool, A., Wiltshire, A., O'Connor, F. M., Stringer, M., Hill, R., Palmieri, J., Woodward, S., de Mora, L., Kuhlbrodt, T., Rumbold, S. T., Kelley, D. I., Ellis, R., Johnson, C. E., Walton, J.,

https://doi.org/10.5194/egusphere-2026-4785
Preprint. Discussion started: 28 August 2026

Abraham, N. L., Andrews, M. B., Andrews, T., Archibald, A. T., Berthou, S., Burke, E., Blockley, E., Carslaw, K., Dalvi, M., Edwards, J., Folberth, G. A., Gedney, N., Griffiths, P. T., Harper, A. B., Hendry, M. A., Hewitt, A. J., Johnson, B., Jones, A., Jones, C. D., Keeble, J., Liddicoat, S., Morgenstern, O., Parker, R. J., Predoi, V., Robertson, E., Siahaan, A., Smith, R. S., Swaminathan, R., Woodhouse, M. T., Zeng, G., and Zerroukat, M.: UKESM1: Description and Evaluation of the U.K. Earth System Model, Journal of Advances in Modeling Earth Systems, 11, 4513–4558, https://doi.org/10.1029/2019MS001739, 2019.

Sigl, M., McConnell, J. R., Layman, L., Maselli, O., McGwire, K., Pasteris, D., Dahl-Jensen, D., Steffensen, J. P., Vinther, B., Edwards, R., Mulvaney, R., and Kipfstuhl, S.: A new bipolar ice core record of volcanism from WAIS Divide and NEEM and implications for climate forcing of the last 2000 years, Journal of Geophysical Research: Atmospheres, 118, 1151–1169, https://doi.org/10.1029/2012JD018603, 2013.

Sigl, M., McConnell, J. R., Toohey, M., Curran, M., Das, S. B., Edwards, R., Isaksson, E., Kawamura, K., Kipfstuhl, S., Krüger, K., Layman, L., Maselli, O. J., Motizuki, Y., Motoyama, H., Pasteris, D. R., and Severi, M.: Insights from Antarctica on volcanic forcing during the Common Era, Nature Clim Change, 4, 693–697, https://doi.org/10.1038/nclimate2293, 2014.

Sigl, M., Winstrup, M., McConnell, J. R., Welten, K. C., Plunkett, G., Ludlow, F., Büntgen, U., Caffee, M., Chellman, N., Dahl-Jensen, D., Fischer, H., Kipfstuhl, S., Kostick, C., Maselli, O. J., Mekhaldi, F., Mulvaney, R., Muscheler, R., Pasteris, D. R., Pilcher, J. R., Salzer, M., Schüpbach, S., Steffensen, J. P., Vinther, B. M., and Woodruff, T. E.: Timing and climate forcing of volcanic eruptions for the past 2,500 years, Nature, 523, 543–549, https://doi.org/10.1038/nature14565, 2015.

Stoffel, M., Khodri, M., Corona, C., Guillet, S., Poulain, V., Bekki, S., Guiot, J., Luckman, B. H., Oppenheimer, C., Lebas, N., Beniston, M., and Masson-Delmotte, V.: Estimates of volcanic-induced cooling in the Northern Hemisphere over the past 1,500 years, Nature Geosci, 8, 784–788, https://doi.org/10.1038/ngeo2526, 2015.

Stoffel, M., Corona, C., Ludlow, F., Sigl, M., Huhtamaa, H., Garnier, E., Helama, S., Guillet, S., Crampsie, A., Kleemann, K., Camenisch, C., McConnell, J., and Gao, C.: Climatic, weather, and socio-economic conditions corresponding to the mid-17th-century eruption cluster, Climate of the Past, 18, 1083–1108, https://doi.org/10.5194/cp-18-1083-2022, 2022.

Stott, P. A., Gillett, N. P., Hegerl, G. C., Karoly, D. J., Stone, D. A., Zhang, X., and Zwiers, F.: Detection and attribution of climate change: a regional perspective, WIREs Climate Change, 1, 192–211, https://doi.org/10.1002/wcc.34, 2010.

Tejedor, E., Steiger, N. J., Smerdon, J. E., Serrano-Notivoli, R., and Vuille, M.: Global hydroclimatic response to tropical volcanic eruptions over the last millennium, Proceedings of the National Academy of Sciences, 118, e2019145118, https://doi.org/10.1073/pnas.2019145118, 2021.

Timmreck, C., Olonscheck, D., Ballinger, A. P., D'Agostino, R., Fang, S.-W., Schurer, A. P., and Hegerl, G. C.: Linearity of the Climate Response to Increasingly Strong Tropical Volcanic Eruptions in a Large Ensemble Framework, https://doi.org/10.1175/JCLI-D-23-0408.1, 2024.

Toohey, M. and Sigl, M.: Volcanic stratospheric sulfur injections and aerosol optical depth from 500 BCE to 1900 CE, Earth System Science Data, 9, 809–831, https://doi.org/10.5194/essd-9-809-2017, 2017.

Toohey, M., Stevens, B., Schmidt, H., and Timmreck, C.: Easy Volcanic Aerosol (EVA v1.0): an idealized forcing generator for climate simulations, Geoscientific Model Development, 9, 4049–4070, https://doi.org/10.5194/gmd-9-4049-2016, 2016.

Toohey, M., Krüger, K., Schmidt, H., Timmreck, C., Sigl, M., Stoffel, M., and Wilson, R.: Disproportionately strong climate forcing from extratropical explosive volcanic eruptions, Nature Geosci, 12, 100–107, https://doi.org/10.1038/s41561-018-0286-2, 2019.

https://doi.org/10.5194/egusphere-2026-4785
Preprint. Discussion started: 28 August 2026

Villalba, R.: Tree-ring and glacial evidence for the medieval warm epoch and the little ice age in southern South America, Climatic Change, 26, 183–197, https://doi.org/10.1007/BF01092413, 1994.

Villalba, R., Lara, A., Boninsegna, J. A., Masiokas, M., Delgado, S., Aravena, J. C., Roig, F. A., Schmelter, A., Wolodarsky, A., and Ripalta, A.: Large-Scale Temperature Changes across the Southern Andes: 20th-Century Variations in the Context of the Past 400 Years, Climatic Change, 59, 177–232, https://doi.org/10.1023/A:1024452701153, 2003.

Villamayor, J., Khodri, M., Fang, S.-W., Jungclaus, J. H., Timmreck, C., and Zanchettin, D.: Sahel Droughts Induced by Large Volcanic Eruptions Over the Last Millennium in PMIP4/Past1000 Simulations, Geophysical Research Letters, 50, e2022GL101478, https://doi.org/10.1029/2022GL101478, 2023.

Volodin, E., Mortikov, E., Gritsun, A., Lykossov, V., Galin, V., Diansky, N., Gusev, A., Kostrykin, S., Iakovlev, N., Shestakova, A., and Emelina, S.: INM INM-CM4-8 model output prepared for CMIP6 CMIP, 2019.

Wang, F., Arseneault, D., Boucher, É., Yu, S., Ouellet, S., Chaillou, G., Delwaide, A., and Wang, L.: Chemical destaining and the delta correction for blue intensity measurements of stained lake subfossil trees, Biogeosciences, 17, 4559–4570, https://doi.org/10.5194/bg-17-4559-2020, 2020.

Wigley, T. M. L., Briffa, K. R., and Jones, P. D.: On the Average Value of Correlated Time Series, with Applications in Dendroclimatology and Hydrometeorology, 1984.

Wilson, R., Anchukaitis, K., Briffa, K. R., Büntgen, U., Cook, E., D'Arrigo, R., Davi, N., Esper, J., Frank, D., Gunnarson, B., Hegerl, G., Helama, S., Klesse, S., Krusic, P. J., Linderholm, H. W., Myglan, V., Osborn, T. J., Rydval, M., Schneider, L., Schurer, A., Wiles, G., Zhang, P., and Zorita, E.: Last millennium northern hemisphere summer temperatures from tree rings: Part I: The long term context, Quaternary Science Reviews, 134, 1–18, https://doi.org/10.1016/j.quascirev.2015.12.005, 2016.

Wilson, R., D'Arrigo, R., Andreu-Hayles, L., Oelkers, R., Wiles, G., Anchukaitis, K., and Davi, N.: Experiments based on blue intensity for reconstructing North Pacific temperatures along the Gulf of Alaska, Climate of the Past, 13, 1007–1022, https://doi.org/10.5194/cp-13-1007-2017, 2017.

Wilson, R., Anchukaitis, K., Andreu-Hayles, L., Cook, E., D'Arrigo, R., Davi, N., Haberbauer, L., Krusic, P., Luckman, B., Morimoto, D., Oelkers, R., Wiles, G., and Wood, C.: Improved dendroclimatic calibration using blue intensity in the southern Yukon, The Holocene, 29, 1817–1830, https://doi.org/10.1177/0959683619862037, 2019.

Wilson, R., Allen, K., Baker, P., Boswijk, G., Buckley, B., Cook, E., D'Arrigo, R., Druckenbrod, D., Fowler, A., Grandjean, M., Krusic, P., and Palmer, J.: Evaluating the dendroclimatological potential of blue intensity on multiple conifer species from Tasmania and New Zealand, Biogeosciences, 18, 6393–6421, https://doi.org/10.5194/bg-18-6393-2021, 2021.

Yukimoto, S., Koshiro, T., Kawai, H., Oshima, N., Yoshida, K., Urakawa, S., Tsujino, H., Deushi, M., Tanaka, T., Hosaka, M., Yoshimura, H., Shindo, E., Mizuta, R., Ishii, M., Obata, A., and Adachi, Y.: MRI MRI-ESM2.0 model output prepared for CMIP6 CMIP, 2019.

Ziehn, T., Chamberlain, M. A., Law, R. M., Lenton, A., Bodman, R. W., Dix, M., Stevens, L., Wang, Y.-P., and Srbinovsky, J.: The Australian Earth System Model: ACCESS-ESM1.5, JSHESS, 70, 193–214, https://doi.org/10.1071/ES19035, 2020.